



Cite this: *J. Anal. At. Spectrom.*, 2023, **38**, 2674

Developing and downscaling a method by HILIC coupled simultaneously to ESIMS and ICPMS to determine the affinity of lanthanide chelating molecules using specific isotope dilution

Marina Amaral Saraiva,^a Pascal E. Reiller,^{ib}^a Cécile Marie^{ib}^b and Carole Bresson^{ib}^{*a}

Recycling minor actinides (Am, Cm and Np) from spent nuclear fuel is considered by a few countries as an important option for a future sustainable nuclear fuel cycle. For this purpose, solvent extraction processes are developed to separate minor actinides, especially from lanthanides and other fission products. The development of fast and powerful analytical methods is essential to acquire the data needed to model these processes and to improve their performances. For this purpose, this study presents the development, validation and application of a new analytical approach based on the simultaneous coupling of hydrophilic interaction chromatography (HILIC) to electrospray ionization mass spectrometry (ESIMS) and inductively coupled plasma mass spectrometry (ICPMS), using specific isotope dilution (SID) as a method of quantification for the determination of the affinity and selectivity of chelating molecules (TPAEN, NM and DTPA) towards lanthanides (Ln). The best separation conditions of ^{nat}Nd and ^{nat}Sm complexes formed with the three molecules were defined. Then, downscaling the separation was investigated, to reduce effluent volumes, the consumption of materials and the time devoted to experiments which are of concern in the nuclear field. The separation was carried out using an amide grafted stationary phase column in isocratic and gradient elution modes depending on the separation format. The separated complexes were online identified and the quantitative distribution of the Ln among the complexes was simultaneously determined owing to our quantification strategy. The results obtained were similar for the three separation formats, allowing us to validate the robustness of the method. By applying this method, the affinity of TPAEN, NM and DTPA present in competition for the complexation reaction with ^{nat}Nd and ^{nat}Sm was further determined in a single step, allowing a quick screening. Both selectivity and affinity of these molecules could be compared to select the most promising candidates. This approach can be advantageously extended to the evaluation of the affinity of various classes of chelating molecules used in very low quantities, towards elements of interest in the fields of energy, toxicology and the environment.

Received 3rd August 2023
 Accepted 12th October 2023

DOI: 10.1039/d3ja00263b

rsc.li/jaas

1. Introduction

In the energy sector, recycling recoverable materials is a societal and economic challenge. Concerning the nuclear fuel cycle, the minor actinides (An) such as americium (Am) and curium (Cm), although representing only 1% by weight of spent nuclear fuel from current light water reactors,¹ are responsible for much of the radiotoxicity and long-term heat load of the final high level waste. That is why following the extraction of uranium (U) and plutonium (Pu) from spent fuel solutions, the selective recovery

of Am and Cm in order to partially or totally recycle them is considered a promising strategy by a few countries.² Hence, several studies are focused on the development of specific molecules to set up dedicated treatment processes, especially for the partitioning of Am.²⁻⁴

The treatment processes developed to ensure the selective recovery of the target radionuclides are mainly based on liquid-liquid extraction. A key step is the design of the extraction/back-extraction molecules that must exhibit high selectivity and affinity towards the elements of interest, requiring the synthesis and the screening of numerous molecules. Two of the major criteria for selecting the candidate molecules are (i) the affinity for the targeted element(s); (ii) the selectivity *versus* impurities or secondary elements to be able to perform separation of intra-group or inter-group elements.

^aUniversité Paris-Saclay, CEA, Service de Physico-Chimie, F-91191, Gif-sur-Yvette Cédex, France. E-mail: carole.bresson@cea.fr

^bUniversité de Montpellier, CEA, DES, ISEC, DMRC, F-30207, Bagnols sur Cèze Cédex, France



In general, the affinity and the selectivity of the molecules are evaluated by combining information obtained from conventional methods such as liquid–liquid extraction, giving distribution coefficients and from solution chemistry techniques, through the thermodynamic and structural characterisation of the complexes formed with the molecules, by time-resolved laser fluorescence spectroscopy (TRLFS), fluorescence spectroscopy, microcalorimetry, potentiometry, infrared and UV-visible spectroscopy, nuclear magnetic resonance (NMR), extended X-ray absorption fine structure spectroscopy (EXAFS) or electrospray ionization mass spectrometry (ESI-MS) using direct introduction of samples.^{5–12} In addition, these experiments are carried out in sequential mode and are often devoted to the characterisation of each complex independently, leading to significant consumption of materials and time, and preventing to assess affinity/selectivity properties when the molecules are in competing complexation reactions towards several elements.

The development of analytical methods allowing the quick determination of the selectivity and the affinity of molecules towards the targeted elements, while reducing the consumption of materials, effluent volumes and the time devoted to the screening experiments, is of great concern for an accelerated and rational research of efficient molecules. To meet this goal, the strategy of this work was based on the simultaneous coupling of hydrophilic liquid chromatography (HILIC) to electrospray ionization mass spectrometry (ESIMS) and inductively coupled plasma mass spectrometry (ICPMS) previously set up in the laboratory.¹³ This powerful approach allows, online and simultaneously, the structural, multi-elemental and isotopic characterization of chemical species coming from the chromatographic separation. Hence, the quantitative distribution of the elements among the complexes formed with the different chelating molecules (CMs) in a sample can be determined, allowing the selectivity and the affinity of the molecules for the elements to be reached, in a single analysis. This approach has been undertaken to determine the selectivity and affinity of two hydrophilic CMs towards natural samarium (^{nat}Sm) and natural neodymium (^{nat}Nd), compared to those of commercial diethylene triamine pentaacetic acid (DTPA) as a reference molecule (Fig. 1). One of the molecules, investigated as potential selective back-extraction reagents of actinides especially for Am/Cm partitioning, contains a diamine bridge and four picolinic acid arms: *N,N,N',N'*-tetrakis[(6-carboxypyridin-2-yl)methyl]ethylenediamine (TPAEN)^{14,15} and

the second new one is a nitrogenous macrocycle (NM) (Fig. 1). Sm and Nd were chosen as analogues of Am and Cm to develop the method in a conventional laboratory, because of their similar physicochemical properties^{16–19} such as similar ionic radius, hard acid character according to the Pearson theory,¹⁶ same +III oxidation state in solution and high coordination numbers.

In the first step, the best HILIC separation conditions of the ^{nat}Sm and ^{nat}Nd complexes formed with the three molecules were defined. To our knowledge, only HILIC separations of gadolinium complexes containing contrast agents based on linear/cyclic polyaminocarboxylic acid derivatives are reported in the literature^{20–30} and our group has also developed the separation of Ln complexes formed with DTPA and EDTA ligands.^{13,31} However, the separation mechanism of HILIC mode is known to be very complex,³² which required developments in order to separate these new sets of complexes. To this end, several stationary phases functionalized with different polar groups were tested in the conventional chromatographic format as well as several mobile phase compositions. An important part of this work was further dedicated to the reduction of the scale of separation to the capillary and to the nano-flow formats while maintaining the performance of the analytical method. The aim was to reduce the consumption of the quantity of materials and molecules used since their synthesis is delicate, a limiting aspect leading to the availability of very few amounts of TPAEN and NM to develop our method. Another aim was to decrease the volume of effluents generated during the analysis, which is of great concern in the nuclear domain.

Then, a method of quantification by specific isotope dilution (SID) was developed and validated, to quantify online and precisely the distribution of ^{nat}Sm and ^{nat}Nd among the separated complexes simultaneously identified by ESIMS. Compared to external calibration, the SID quantification method allows the reduction of the material consumption and analysis time and makes the results more precise because the errors resulting from the analytical procedure can be corrected mathematically and quantitatively.³³ Briefly, SID is based on the measurement of isotope ratios in a sample whose analyte isotopic composition is altered by the addition of a known amount of an isotopically modified analyte (spike).³⁴ The advantage of SID is that once the isotopic equilibrium between the sample and the spike(s) is achieved, the physical effects induced by the matrix, potential species loss (*e.g.*, incomplete extraction) or transformation (*e.g.* oxidation and/or reduction) during the

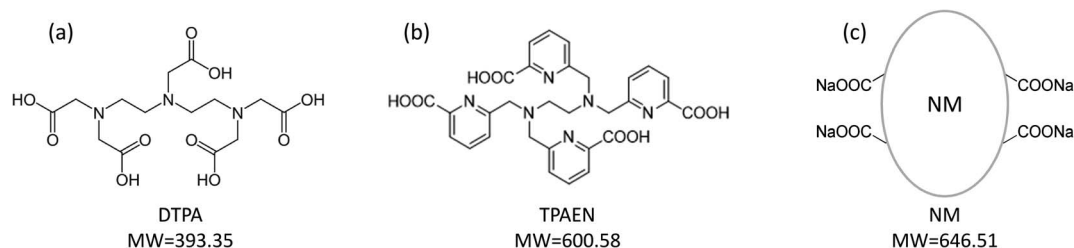


Fig. 1 Chemical structures of DTPA (a), TPAEN (b) and NM (c).



analytical process does not influence the method accuracy, owing to the measurement of isotopic ratios rather than the absolute or relative signals as for conventional analytical methods.³³ In the nuclear domain, the quantification of Ln and/or An has been widely developed using non-specific isotopic dilution, to measure elemental concentrations with low uncertainties.^{35–39} To our knowledge, the separation, online identification and quantification of Ln complexes by HILIC-ESIMS-SID-ICPMS has never been reported in the literature.

By applying this approach, the affinity of the three chelating molecules for ^{nat}Sm and ^{nat}Nd could be determined online and in a single analysis. For this, several stoichiometric ratios of TPAEN, NM and DTPA were added in competition for the complexation reaction of ^{nat}Sm and ^{nat}Nd in the samples, leading to the formation of the complexes in different proportions according to the selectivity and affinity of the molecules towards the Ln. The benefits provided by our approach compared to studies reported in the literature have been highlighted.

2. Experimental section

2.1. Chemicals and reagents

All the aqueous solutions and mobile phases were prepared with ultrapure water (18.2 MΩ cm, Merck Millipore, Guyancourt – France). Acetonitrile (ACN, CH₃CN, LC-MS grade), formic acid (Normapur grade) and ammonia solution 22% (v/v) were purchased from VWR Prolabo (Briare-le-Canal, France). Ammonium acetate (NH₄CH₃CO₂) was supplied by Sigma Aldrich (Saint Quentin Fallavier, France).

Standard solutions (1000 mg L⁻¹ in HNO₃ 2% w/w) of ^{nat}Sm and ^{nat}Nd were provided by SCP SciencePlasmaCal (Courtaboeuf, France) and standard solutions of bismuth (²⁰⁹Bi) and indium (¹¹⁵In) were from the Spex Certiprep Group (Longjumeau, France). Nitric acid (67–69% w/w, NORMATOM®, VWR, Fontenay-sous-Bois, France) was used to prepare HNO₃ 2% w/w in ultrapure water. The isotopically enriched oxide powders ¹⁴⁷Sm₂O₃ and ¹⁴⁵Nd₂O₃ were from Euriso-top (Saint-Aubin CEDEX, France) with the isotope abundance of respectively 94.0% and 87.1% as provided by the manufacturer's certificate, but without uncertainties. The standard reference materials, Sm – 3147a and Nd – 3135a (NIST, Gaithersburg, US), both at 8.52 ± 0.02 mg g⁻¹ in HNO₃ 10% w/w, were used for the quantification of the spike solutions by thermal ionization mass spectrometry (TIMS).

Diethylene triamine pentaacetic acid (DTPA, C₁₄H₂₃O₁₀N₃, purity ≥ 98%) was provided by Sigma Aldrich (Saint Quentin Fallavier, France), *N,N,N',N'*-tetrakis[[6-carboxypyridin-2-yl)methyl]ethylenediamine (TPAEN)^{14,15} and the nitrogenous macrocycle (NM) were synthesized, characterized and supplied by the LCIS team (Université de Montpellier, DES/ISEC/DMRC, CEA Marcoule, France).

2.2. Preparation of stock, intermediate, contact and control solutions, samples and controls

2.2.1. Stock solutions of chelating molecules, natural lanthanides and spikes. Stock solutions of the chelating

molecules were prepared by dissolving the appropriate amount of powder in ultrapure water to obtain 3.0 × 10⁻³ mol L⁻¹ for TPAEN, NM and DTPA.

The commercial standard solutions of ^{nat}Sm and ^{nat}Nd were diluted in HNO₃ 2% w/w to obtain individual stock solutions at 5.0 × 10⁻³ mol L⁻¹.

The stock solutions of the spikes isotopically enriched in ¹⁴⁷Sm and ¹⁴⁵Nd (^{spike}Ln) were prepared by dissolving the appropriate amount of the corresponding enriched Ln₂O₃ oxide powders (¹⁴⁷Sm₂O₃ and ¹⁴⁵Nd₂O₃) in HNO₃ 2% w/w to obtain a concentration of each isotope of 5.1 × 10⁻³ mol L⁻¹.

2.2.2. Intermediate solutions. One intermediate solution containing ^{nat}Sm and ^{nat}Nd was prepared weekly by diluting the corresponding stock solutions in ultrapure water to obtain a concentration of 5.0 × 10⁻⁴ mol L⁻¹ for each Ln, which was measured offline by ICP-MS.

2.2.3. Contact solutions. The contact solutions were prepared in polypropylene tubes as follows:



where 100 μL (for conventional separation format) or 50 μL (for capillary and nano-flow separation formats) of the ^{nat}Sm and ^{nat}Nd intermediate solution were added to the required volume of ¹⁴⁷Sm and ¹⁴⁵Nd spike solutions to reach ¹⁴⁷Sm/¹⁵²Sm and ¹⁴⁵Nd/¹⁴²Nd ratios equal to 1, by considering the most abundant natural isotopes ¹⁵²Sm and ¹⁴²Nd. The equilibration between ^{nat}Ln (^{nat}Sm + ^{nat}Nd) and ^{spike}Ln (¹⁴⁷Sm + ¹⁴⁵Nd) solutions is a critical step in the SID technique to carry out accurate quantitative measurements.⁴⁰ In order to ensure the equilibration, the blends containing all the lanthanides (Ln_T = ^{nat}Ln + ^{spike}Ln) were stirred manually for 5 minutes. Adequate volume of the stock solutions of each chelating molecule was added afterwards to obtain different stoichiometric ratios of the three CMs (x:y:z) compared to those of the Ln_T which was fixed, as reported in Table 1. The pH of each contact solution was adjusted to 1 by adding around 1 μL of ammonia solution (22% v/v).

2.2.4. Control solutions. Three control solutions were prepared as previously but only one of each CM was added to ensure the complexation of all the lanthanides (Ln_T), according to ^{nat}Ln + ^{spike}Ln + 4CM, with the CM being TPAEN or NM or DTPA. Hence, the CM stoichiometric ratio was equimolar compared to this of Ln_T, being the sum of one equivalent of each natural and spike Ln, as can be seen in Table 1. These control solutions were required to control and calculate the chromatographic recovery of the Ln after each separation run of the samples containing the three CMs in different proportions and also to validate the SID method.

2.2.5. Samples and controls. The following day, the contact and control solutions were diluted by a factor of 22 in the mobile phase to obtain samples and controls with concentrations of ^{nat}Sm and ^{nat}Nd consistent with the separation format (Table 1).

Samples 1, 2, 3 and 4 contained different CM stoichiometric ratios compared to this of Ln_T, being one equivalent of each natural and enriched Ln, according to Ln_T:xTPAEN:yNM:zDTPA. The composition of each sample was 4:2.5:1.4:0.1



Table 1 Composition of the controls and samples according to the format of the separation, with $x : y : z$ being the stoichiometric ratios of the chelating molecules compared to this of the Ln_T . The experimental concentrations obtained from the weight of the Ln and the CM solutions are given in brackets (mol L^{-1})

Format		Ln_T^a	$x\text{TPAEN}$	$y\text{NM}$	$z\text{DTPA}$
Conventional	Control 1	4 ($1.1 \times 10^{-5} \text{ mol L}^{-1}$)	4 ($1.7 \times 10^{-5} \text{ mol L}^{-1}$)	0	0
	Control 2	4 ($1.2 \times 10^{-5} \text{ mol L}^{-1}$)	0	4 ($1.8 \times 10^{-5} \text{ mol L}^{-1}$)	0
	Control 3	4 ($1.1 \times 10^{-5} \text{ mol L}^{-1}$)	0	0	4 ($1.7 \times 10^{-5} \text{ mol L}^{-1}$)
	Sample 1	4 ($1.1 \times 10^{-5} \text{ mol L}^{-1}$)	2.5 ($3.0 \times 10^{-5} \text{ mol L}^{-1}$)	1.4 ($6.1 \times 10^{-6} \text{ mol L}^{-1}$)	0.1 ($4.5 \times 10^{-7} \text{ mol L}^{-1}$)
	Sample 2	4 ($1.2 \times 10^{-5} \text{ mol L}^{-1}$)	1.4 ($6.5 \times 10^{-6} \text{ mol L}^{-1}$)	2.5 ($1.1 \times 10^{-5} \text{ mol L}^{-1}$)	0.1 ($4.6 \times 10^{-7} \text{ mol L}^{-1}$)
	Sample 3	4 ($1.0 \times 10^{-5} \text{ mol L}^{-1}$)	1.8 ($7.4 \times 10^{-6} \text{ mol L}^{-1}$)	1.8 ($7.6 \times 10^{-6} \text{ mol L}^{-1}$)	0.4 ($1.3 \times 10^{-6} \text{ mol L}^{-1}$)
	Sample 4	—	—	—	—
Capillary	Control 1	4 ($2.2 \times 10^{-6} \text{ mol L}^{-1}$)	4 ($3.6 \times 10^{-6} \text{ mol L}^{-1}$)	0	0
	Control 2	4 ($2.3 \times 10^{-6} \text{ mol L}^{-1}$)	0	4 ($3.6 \times 10^{-6} \text{ mol L}^{-1}$)	0
	Control 3	4 ($2.2 \times 10^{-6} \text{ mol L}^{-1}$)	0	0	4 ($3.5 \times 10^{-6} \text{ mol L}^{-1}$)
	Sample 1	4 ($3.1 \times 10^{-6} \text{ mol L}^{-1}$)	2.5 ($1.6 \times 10^{-5} \text{ mol L}^{-1}$)	1.4 ($1.8 \times 10^{-6} \text{ mol L}^{-1}$)	0.1 ($1.4 \times 10^{-7} \text{ mol L}^{-1}$)
	Sample 2	4 ($3.6 \times 10^{-6} \text{ mol L}^{-1}$)	1.4 ($2.0 \times 10^{-6} \text{ mol L}^{-1}$)	2.5 ($3.6 \times 10^{-6} \text{ mol L}^{-1}$)	0.1 ($1.4 \times 10^{-7} \text{ mol L}^{-1}$)
	Sample 3	4 ($2.9 \times 10^{-6} \text{ mol L}^{-1}$)	1.8 ($2.0 \times 10^{-6} \text{ mol L}^{-1}$)	1.8 ($2.0 \times 10^{-6} \text{ mol L}^{-1}$)	0.4 ($4.5 \times 10^{-7} \text{ mol L}^{-1}$)
	Sample 4	4 ($2.6 \times 10^{-6} \text{ mol L}^{-1}$)	1.3 ($1.3 \times 10^{-6} \text{ mol L}^{-1}$)	1.3 ($1.2 \times 10^{-6} \text{ mol L}^{-1}$)	1.3 ($1.3 \times 10^{-6} \text{ mol L}^{-1}$)
Nano	Control 1	4 ($5.8 \times 10^{-6} \text{ mol L}^{-1}$)	4 ($9.4 \times 10^{-6} \text{ mol L}^{-1}$)	0	0
	Control 2	4 ($5.7 \times 10^{-6} \text{ mol L}^{-1}$)	0	4 ($9.1 \times 10^{-6} \text{ mol L}^{-1}$)	0
	Control 3	4 ($5.9 \times 10^{-6} \text{ mol L}^{-1}$)	0	0	4 ($9.3 \times 10^{-6} \text{ mol L}^{-1}$)
	Sample 1	4 ($6.0 \times 10^{-6} \text{ mol L}^{-1}$)	2.5 ($5.7 \times 10^{-6} \text{ mol L}^{-1}$)	1.4 ($3.5 \times 10^{-6} \text{ mol L}^{-1}$)	0.1 ($2.6 \times 10^{-7} \text{ mol L}^{-1}$)
	Sample 2	4 ($6.0 \times 10^{-6} \text{ mol L}^{-1}$)	1.4 ($3.0 \times 10^{-6} \text{ mol L}^{-1}$)	2.5 ($6.0 \times 10^{-6} \text{ mol L}^{-1}$)	0.1 ($2.1 \times 10^{-7} \text{ mol L}^{-1}$)
	Sample 3	4 ($5.9 \times 10^{-6} \text{ mol L}^{-1}$)	1.8 ($4.1 \times 10^{-6} \text{ mol L}^{-1}$)	1.8 ($4.0 \times 10^{-6} \text{ mol L}^{-1}$)	0.4 ($9.1 \times 10^{-7} \text{ mol L}^{-1}$)
	Sample 4	4 ($6.1 \times 10^{-6} \text{ mol L}^{-1}$)	1.3 ($3.1 \times 10^{-6} \text{ mol L}^{-1}$)	1.3 ($3.0 \times 10^{-6} \text{ mol L}^{-1}$)	1.3 ($3.1 \times 10^{-6} \text{ mol L}^{-1}$)

$$^a \text{Ln}_T = \text{natLn} + \text{spikeLn}.$$

(sample 1), 4 : 1.4 : 2.5 : 0.1 (sample 2), 4 : 1.8 : 1.8 : 0.4 (sample 3) and 4 : 1.3 : 1.3 : 1.3 (sample 4). Controls 1, 2 and 3 contained one of each CM in equimolar stoichiometric ratios with respect to this of Ln_T . The composition of each control was Ln_T :4TPAEN (control 1), Ln_T :4NM (control 2), Ln_T :4DTPA (control 3), with $\text{Ln}_T = 1^{\text{nat}}\text{Sm} + 1^{\text{nat}}\text{Nd} + 1^{\text{spike}}\text{Sm} + 1^{\text{spike}}\text{Nd}$. The samples and controls were prepared and injected in duplicate in the column after 1 hour. The stock, intermediate and contact solutions were stored in a refrigerator at 4–5 °C for a maximum of one month.

Additional five contact solutions containing equimolar ratios of the CM regarding this of the Ln_T , 4 : 1.33 : 1.33 : 1.33 (sample 4) were prepared and the pH was adjusted between 1 and 10 (1.36, 2.85, 5.31, 6.93 and 9.56) with ammonia solution 22% (v/v). The solutions were left overnight and diluted into the working mobile phase the next day to obtain the corresponding samples.

2.3. Instrumentation

The chromatographic separations in conventional format were carried out using an ultimate 3000 UHPLC⁺ system (Dionex/ThermoFisher Scientific, Courtaboeuf, France), consisting of a degasser, a dual RS pump, an RS autosampler, a column compartment and an RS diode array detector. The ultimate 3000 RSLCnano System (ThermoFisher Scientific, Courtaboeuf, France) was composed of a pump module equipped with pro-flow and capillary flowmeters.

A triple quadrupole TSQ Quantum Ultra™ mass spectrometer (Thermo Fisher Scientific, San Diego CA, USA) equipped with an H-ESI II ionisation probe was used for the simultaneous coupling to the separations in conventional and capillary

formats. Mass spectra were registered in full scan mode (m/z 300–800) and in selected ion monitoring mode (SIM) by considering the most abundant m/z ratio of the isotopic pattern associated with the Ln-complexes, namely $m/z = 743$ for the Ln-TPAEN complexes, $m/z = 702$ for the Ln-NM complexes and $m/z = 537$ for the Ln-DTPA complexes, with Ln being natural and spike Sm and Nd (spectral width $m/z \pm 12$). The data were processed with Xcalibur software.

The ICPMS instrument used for the simultaneous coupling of the separations carried out in conventional format was an XSeriesII (Thermo Electron SAS, Courtaboeuf, France) equipped with platinum skimmer and sampler cones, a MicroMist nebulizer operating at 400 $\mu\text{L min}^{-1}$ (Thermo Scientific BRE0009386) and a quartz cyclonic spray chamber (Thermo Scientific 1317080) thermostated at 3 °C. The data were processed with PlasmaLab software.

An 8800 Triple Quadrupole ICPMS (Agilent, Courtaboeuf, France) was also used for the coupling experiments associated with the chromatographic downscaling, owing to its better sensitivity when working at micro flow rates. A total consumption micro nebulizer operating 10 $\mu\text{L min}^{-1}$ (Agilent G3280-80602) equipped with a single pass spray chamber (Agilent G3280-80603 in quartz material) was used for the coupling experiments in capillary and nano-flow rate formats. The data were processed with Mass Hunter software.

In order to prevent any carbon deposition on the cones due to the use of acetonitrile, oxygen was injected at 8 mL min^{-1} in the plasma after the spray chamber when using the ICPMS XSeriesII^{13,31} and O_2/Ar mix at 0.5 L min^{-1} of for the ICPMS 8800 TQ.



Table 2 Operating ESI-QqQ-MS and ICPMS parameters according to the separation format. The ESI mass spectrometer was used with the ICPMS XSeriesII for coupling in conventional and capillary formats and only ICPMS 8800TQ was coupled for nano-flow format

	ESIMS TSQ Quantum Ultra		ICPMS XSeriesII	ICPMS 8800 TQ
Spray voltage	−3.7 kV	Plasma gas flow rate	14 L min ^{−1}	15 L min ^{−1}
Capillary transfer temperature	250 °C	Auxiliary gas flow rate	0.9 L min ^{−1}	0.9 L min ^{−1}
Vaporisation temperature	150 °C	Nebuliser gas flow rate	0.8 L min ^{−1}	0.7 L min ^{−1}
Sheath gas pressure	15 a.u.	Dilution gas flow rate	8 mL min ^{−1} (O ₂)	0.5 L min ^{−1} (O ₂ /Ar 20%/80%)
Auxiliary gas pressure	35 a.u.	Nebulizer liquid flow rate	130 μL min ^{−1}	0.3 μL min ^{−1}
Scan width	20 (<i>m/z</i>)	Tip material	Platinum	Platinum
Scan time	0.7 s	Sampler cone diameter (Pt)	1.0 mm	1.2 mm
FWHM	0.5	Plasma power	1550 W	1550 W
		Dwell time	30 ms	10 ms
		Monitored isotopes	¹⁴² Nd, ¹⁴⁵ Nd, ¹⁴⁷ Sm, ¹⁵² Sm, ²⁰⁹ Bi ^a	¹⁴² Nd, ¹⁴⁵ Nd, ¹⁴⁷ Sm, ¹⁵² Sm, ¹¹⁵ In ^a

^a Used as internal standards.

The operating ESI-QqQ-MS, ICP-MS XseriesII and 8800 TQ parameters are summarized in Table 2.

2.4. Chromatographic conditions

The separation of the Ln complexes was developed in the conventional format and further transposed to the capillary flow format, before reaching the nano-flow format. The physicochemical properties and the dimensions of the columns used in the different formats are summarized in Table 3.

The chromatographic parameters: retention factor (*k'*), selectivity and resolution factors (α and R_s) were calculated to evaluate the performance of the different columns.⁴¹

The retention factor (*k'*) was calculated according to eqn (1):

$$k' = \frac{(t_R - t_0)}{t_0} \quad (1)$$

where t_R is the retention time (min) of each complex determined by HILIC-ESIMS and t_0 is the void time of the toluene as an unretained marker (10^{-4} mol L^{−1}, $V_{inj} = 1$ μL), determined by HILIC-UV/VIS at 254 nm.

The selectivity factor (α) was calculated based on eqn (2) and the resolution factor (R_s) based on eqn (3):

$$\alpha = \frac{k'_2}{k'_1} \quad (2)$$

$$R_s = 1.18 \times \frac{t_{R2} - t_{R1}}{w_{0.5h1} - w_{0.5h2}} \quad (3)$$

Analyte 2 was more retained than analyte 1 and $w_{0.5h}$ corresponds to full-width at half-maximum of each peak.

The chromatographic conditions for each separation format are presented in Table 4.

2.5. Simultaneous coupling of HILIC to ESIMS and ICPMS

The instrumental configuration of the simultaneous coupling of HILIC in conventional separation format to ESIMS and the

ICPMS XSeriesII was previously developed in the laboratory.¹³ By applying this setup, the outflow from the column was split to enter the ESIMS with a flow rate of 295 μL min^{−1} (98.3%) and 5 μL min^{−1} for the flow entering the ICPMS (1.7%). A make-up made of 2% HNO₃ w/w and containing 10 ppb of ²⁰⁹Bi as internal standard was added to the flow entering the ICPMS, with a flow rate of 140 μL min^{−1}. More details regarding the instrumental conditions are provided in ref. 13.

For the simultaneous coupling involving the separation downscaling, the outflow from the capillary column was split to simultaneously enter the ESIMS with a flow rate of 4.70 μL min^{−1} (94%) and the ICPMS with a flow rate of 0.30 μL min^{−1} (6%). In the case of nano-flow format experiments, the capillary was only coupled to ICPMS with a flow rate of 0.30 μL min^{−1}.

The torch position, the nebulizer and auxiliary gas as well as the optical lens system were optimized daily using a mixed solution of ^{nat}Sm–^{nat}Nd–DTPA. ²⁰⁹Bi solution at 10 ppb in 2% HNO₃ w/w was used as an internal standard for the conventional separation format and ¹¹⁵In at 50 ppb was the internal standard added in the mobile phase of the capillary and nano-flow separations, to monitor the signal stability before and during the analyses.

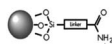
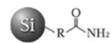
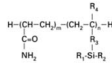
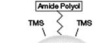
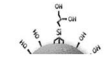
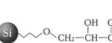
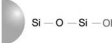
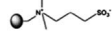
2.6. Development of the quantification method by specific isotope dilution (SID)

A dedicated quantification method using SID was developed and validated based on the mathematical model provided in the literature,⁴² to quantify precisely and online the distribution of ^{nat}Sm and ^{nat}Nd among the complexes coming from the separations.

In the first step, the concentration of ¹⁴⁵Nd and ¹⁴⁷Sm in the stock solutions of the spikes was determined based on thermal ionization mass spectrometry (TIMS), which was used to measure isotopic ratios of mixed solutions made of the spikes and standard reference material of ^{nat}Sm and ^{nat}Nd. The precise concentration of ¹⁴⁵Nd and ¹⁴⁷Sm was further quantified, by applying the methods developed by the CEA-LANIE.^{43,44} The



Table 3 Physico-chemical properties and dimensions of the columns tested. The columns with the best performance in conventional, capillary and nano-flow formats are shown in bold^a

Name (manufacturer)	Dimension (mm); particle size (μm); pore size (Å)	Material support	Stationary phase functionalization	Functional group
ACQUITY BEH Amide (Waters)	150 × 2.1; 1.7; 130	BEH silica	Amide	
InertSustain Amide (GLSciences)	150 × 0.3; 3.0; 100	Ultra-pure silica	Amide	
InertSustain Amide (GLSciences)	150 × 0.075; 3; 100	Ultra-pure silica	Amide	
Accucore Amide (ThermoFisher)	100 × 2.1; 2.6; 150	Ultra-pure silica	Amide	
TSKgel Amide-80 (Tosoh)	150 × 2.1; 3.0; 80	Silica	Amide	
BioZen Glycan (Phenomenex)	150 × 2.1; 2.6; 100	n.a	Amide polyol	
Triart Diol HILIC (YMC)	150 × 2.1; 1.9; 120	Organic/inorganic hybrid silica	Diol	
Luna HILIC (Phenomenex)	100 × 2.1; 3.0; 200	Silica	Diol	—
Inertsil HILIC (GL Science)	100 × 2.1; 3.0; 100	Ultra-pure silica	Diol	
Inertsil Diol (GL Science)	150 × 2.1; 3.0; 100	Ultra-pure silica	Diol	—
Acclaim HILIC-10 (ThermoFisher)	150 × 2.1; 3.0; 120	Ultra-pure silica	Proprietary group	Proprietary
Acclaim WCX-1 (ThermoFisher)	150 × 2.1; 5.0; 120	Ultra-pure silica	Mixed mode	—
Acclaim Trinity P1 (ThermoFisher)	150 × 2.1; 3.0; 300	Hybrid silica	Mixed mode	—
Hypersil Gold HILIC (ThermoFisher)	100 × 2.1; 1.9; 175	Ultra-pure silica	Polyethylenimine	—
Hypersil Gold silica (ThermoFisher)	100 × 2.1; 1.9; 175	Highly pure deactivated silica	Silica	—
Pack Sil (YMC)	100 × 2.1; 3.0; 120	Ultra-pure silica	Silica	—
Triart Sil (YMC)	100 × 2.1; 3.0; 120	Organic/inorganic hybrid silica	Silica	—
Luna silica (Phenomenex)	100 × 2.1; 3.0; 100	Ultra-high purity silica	Silica	
ACQUITY BEH HILIC (Waters)	150 × 2.1; 1.7; 150	BEH silica	Silica	—
Syncronis HILIC (ThermoFisher)	150 × 2.1; 5.0; 100	Ultra-pure silica	Zwitterionic (sulfobetaine)	—
ZIC-HILIC (Merck)	150 × 2.1; 3.5; 100	Polymeric	Zwitterionic (sulfobetaine)	

^a BEH – bridged ethylene hybrid; n.a — not available.

measured concentrations of ¹⁴⁵Nd and ¹⁴⁷Sm were 1067.01 μg g⁻¹ ± 0.94 and 984.22 μg g⁻¹ ± 0.41 respectively and were taken into account for the SID calculations.

The samples were spiked with known amounts of ¹⁴⁵Nd and ¹⁴⁷Sm to achieve ¹⁴⁵Nd/¹⁴²Nd and ¹⁴⁷Sm/¹⁵²Sm isotope ratios

equal to one in the blend samples. For this purpose, the mass of each spike stock solution to add to the sample was calculated based on eqn (4) (example provided here for ¹⁴⁵Nd spike solely).

$$M_S^{145} = \frac{(\text{Nd}^{142} \times m_x) / F^{145/142}}{C_S^{145}} \quad (4)$$

Table 4 Best HILIC separation conditions for the three separation formats

Separation format	Conventional	Capillary	Nano
Mobile phase	74/26 (v/v) ACN/H ₂ O + 0.5% v/v formic acid + 15 mmol L ⁻¹ NH ₄ CH ₃ CO ₂	74/26 (v/v) ACN/H ₂ O + 0.5% v/v formic acid + 10 mmol L ⁻¹ NH ₄ CH ₃ CO ₂	Solvent A: 60/40 (v/v) ACN/H ₂ O + 0.5% v/v formic acid + 7.5 mmol L ⁻¹ NH ₄ CH ₃ CO ₂ Solvent B: 90/10 (v/v) ACN/H ₂ O + 0.5% v/v formic acid + 7.5 mmol L ⁻¹ NH ₄ CH ₃ CO ₂
Elution mode	Isocratic	Isocratic	Gradient 0–0.5 min: 75% B 0.5–3.0 min: 70% B 3.0–6.5 min: 55% B 6.5–25.0 min: 45% B
Injection volume	3 μL	1 μL	0.050 μL
Flow rate	300 μL min ⁻¹	5 μL min ⁻¹	0.3 μL min ⁻¹
Sampler temperature	22 ± 1 °C		
Column temperature	40 ± 1 °C	22 ± 1 °C	22 ± 1 °C
Separation time	20 min	20 min	25 min



where M_s^{145} , mass of ^{145}Nd spike solution added into the sample (g); Nd^{142} , expected concentration of ^{142}Nd in the sample ($\mu\text{g kg}^{-1}$); m_s , sample mass (g); $F^{145/142}$, ratio of the abundance of ^{145}Nd in the spike solution and the natural abundance of ^{142}Nd ; C_s^{145} , concentration of the ^{145}Nd in the spike solution ($\mu\text{g kg}^{-1}$).

The natural abundances of the considered ^{152}Sm and ^{142}Nd isotopes were 26.749 and 27.152% as reported by the Internal Union of Pure and Applied Chemistry.⁴⁵ The abundances of ^{145}Nd and ^{147}Sm in the spike solutions were 87.1% and 94.0% as provided by the manufacturer's certificate.

The $^{\text{nat}}\text{Sm}$ and $^{\text{nat}}\text{Nd}$ contained in the separated complexes were further online quantified based on the elution profiles registered by ICPMS, by monitoring the signal of Sm and Nd isotopes needed for this study as given in Table 2. The integration of the total area of the chromatographic peaks corresponding to the Ln complexes formed with the three chelating molecules in different proportions, combined with the application of SID allowed determination of the quantitative distribution of $^{\text{nat}}\text{Sm}$ and $^{\text{nat}}\text{Nd}$ among the different complexes.

The measured $^{145}\text{Nd}/^{142}\text{Nd}$ and $^{147}\text{Sm}/^{152}\text{Sm}$ natural isotopic ratios were corrected with the mass bias factor (k), determined daily before each analytical procedure, using eqn (5).

$$k = R_r/R_m \quad (5)$$

where R_r and R_m are the reference isotopic ratios provided by IUPAC and the measured isotopic ratios for a given pair of isotopes.

The concentration of $^{\text{nat}}\text{Nd}$ and $^{\text{nat}}\text{Sm}$ in each separated complex was calculated based on eqn (6).

$$C^{\text{nat}} = C_{\text{spike}} \times \frac{m_{\text{spike}}}{m_{\text{nat}}} \times \frac{Aa_{\text{spike}} - R_m \left(\frac{a}{b}\right) \times Ab_{\text{spike}}}{R_m \left(\frac{a}{b}\right) \times Ab_{\text{nat}} - Aa_{\text{nat}}} \times MM_{\text{nat}} \quad (6)$$

where C^{nat} , concentration of $^{\text{nat}}\text{Nd}$ or $^{\text{nat}}\text{Sm}$ ($\mu\text{g g}^{-1}$); C_{spike} , concentration of ^{145}Nd or ^{147}Sm in the spike solution ($\mu\text{g g}^{-1}$); m_{spike} , mass of the ^{145}Nd or ^{147}Sm in the spike solution (g); m_{nat} , mass of $^{\text{nat}}\text{Nd}$ or $^{\text{nat}}\text{Sm}$ in the sample (g); Aa_{spike} , isotopic abundance (%) of each isotope ($a = ^{145}\text{Nd}$ or ^{147}Sm) in the spike solution; Ab_{spike} , isotopic abundance (%) of each isotope ($b = ^{142}\text{Nd}$ or ^{152}Sm) in the spike solution; Aa_{nat} , isotopic abundance (%) of each isotope ($a = ^{145}\text{Nd}$ or ^{147}Sm) in the sample solution; Ab_{nat} , isotopic abundance (%) of each isotope ($b = ^{142}\text{Nd}$ or ^{152}Sm) in the sample solution; $R_m \left(\frac{a}{b}\right)$, measured isotope ratio based on the chromatographic peak integration of the corresponding complex; MM_{nat} , molar mass of $^{\text{nat}}\text{Nd}$ or $^{\text{nat}}\text{Sm}$ (g mol^{-1}).

The limit of detection (LOD) and limit of quantification (LOQ) of $^{\text{nat}}\text{Sm}$ and $^{\text{nat}}\text{Nd}$ -DTPA complexes were determined based on the common method using the calibration curve applying eqn (7).^{46,47}

$$\text{LOD or LOQ} = \frac{F \times \text{SD}}{b} \quad (7)$$

where F , factor of 3 and 10 for LOD and LOQ respectively; SD , standard deviation of ordinate intercept ($n = 3$); b , slope of the calibration curve ($n = 3$).

The LOD and LOQ obtained by nano-HILIC-ICPMS were 3.6 and 12.1 $\mu\text{g kg}^{-1}$ for the $^{\text{nat}}\text{Sm}$ complex and 4.9 and 16.6 $\mu\text{g kg}^{-1}$ for the $^{\text{nat}}\text{Nd}$ complex, respectively.

3. Results and discussion

3.1. Definition of the conditions for separating the Ln complexes in conventional format

3.1.1. Selectivity of different polar stationary phases.

Lanthanide complexes are known to be difficult to separate due to their very close physicochemical properties.⁴⁸ Because of HILIC features,^{32,49} this separation mode is well suited for the separation of such complexes by involving polar stationary phases⁵⁰ and hydro-organic mobile phases, which are moreover compatible with both ESIMS and ICPMS detection conditions.^{51–53}

HILIC separations of Ln (Er, Eu, Gd, and Nd) with strong chelating molecules such as DTPA and EDTA have been previously investigated^{13,31} and our first tests in this work showed that the $^{\text{nat}}\text{Sm}/^{\text{nat}}\text{Nd}$ -DTPA complexes were more retained than the complexes containing NM and TPAEN molecules. Hence, our efforts were first focused on the screening of the selectivity of several columns to separate $^{\text{nat}}\text{Sm}$ and $^{\text{nat}}\text{Nd}$ complexes of NM and TPAEN.

For all the columns, a reference mobile phase composed of 70/30 (v/v) ACN/H₂O containing 15 mmol L⁻¹ NH₄CH₃CO₂ and 0.5% formic acid was initially used and eluted in isocratic mode.¹³ It must be noted that using Luna HILIC, Acclaim Mixed-mode and Biozen Glycan columns, NM and TPAEN complexes co-eluted or were not observed, even with different mobile phase compositions. Therefore, these columns were not selected for the rest of the study. The chromatographic parameters such as retention factor (k'), selectivity factor (α) and resolution factor (R_s) are shown in Table 5. From this table, it can be seen that the TPAEN complexes were well separated from the NM complexes, with selectivity factors between 1.55 and 11.17, except for the Acclaim Trinity column with a value of 1.08. In all cases, NM complexes were more retained than TPAEN complexes with the highest retention factors of NM complexes ranging from 13.5 to 40. The particularly high retention factors obtained with the most polar non-grafted silica columns as well as with the ZIC-HILIC, the Acclaim Trinity or the TSK Gel Amide columns, led us to also exclude these columns. In addition, most of the columns were not selective enough in these conditions to separate efficiently the complexes containing the same molecule, namely the pairs $^{\text{nat}}\text{Sm}$ -TPAEN/ $^{\text{nat}}\text{Nd}$ -TPAEN and $^{\text{nat}}\text{Sm}$ -NM/ $^{\text{nat}}\text{Nd}$ -NM, as for the Triart HILIC or the Acclaim HILIC-10 columns, with α around 1. Except for the ACQUITY UPLC BEH Amide, resolution factors lower than 0.1 to separate the peaks of $^{\text{nat}}\text{Sm}$ -TPAEN and $^{\text{nat}}\text{Nd}$ -TPAEN were obtained for all the columns under the reference conditions.

Finally, the ACQUITY UPLC BEH Amide (150 × 2.1 mm; 1.7 μm) column was selected since it led to the best compromise between acceptable retention factors, satisfying separation of





Table 5 Chromatographic parameters (k' , α_j and R_S) calculated for the separation of TPAEN and NM complexes with stationary phases grafted by different polar functional groups, using a mobile phase composition of 70/30 (v/v) ACN/H₂O, containing 15 mmol L⁻¹ NH₄CH₃CO₂ and 0.5% formic acid^a

Stationary phase functionalization	Amide		Diol				Exclusive				Polyethyl-enimine				Amide polyol				Bare silica				Hybrid silica				Zwitterionic					
	ACQUITY		TSK Gel		Triart Luna		Inerstil Luna		Inerstil Luna		Acclaim Mixed-10 mode		Acclaim Mixed-10 mode		Hypersil Gold		Biozen Glycan		Hypersil Gold		Hypersil YMC Pack Sil		Luna Silica Sil		YMC Triart BEH		Synchronis ZIC-HILIC		YMC Triart BEH		Synchronis ZIC-HILIC	
	UPLC	BEH	Accucore Amide-80	HILIC	HILIC	HILIC	HILIC	HILIC	Diol	Acclaim HILIC-10 mode	Acclaim HILIC-10 mode	Trinity P1	Hypersil Gold	Hypersil Glycan	Hypersil Gold	Hypersil YMC Pack Sil	Luna Silica Sil	YMC Triart BEH	YMC Triart BEH	YMC Triart BEH	YMC Triart BEH	Luna Silica Sil	YMC Triart BEH	YMC Triart BEH	Synchronis ZIC-HILIC	Synchronis ZIC-HILIC	YMC Triart BEH	Synchronis ZIC-HILIC				
k'	Sm-TPAEN	2.93	0.93	1.09	1.02	1.01	—	1.13	1.04	1.02	—	1.01	1.03	ND	1.01	1.02	1.01	1.04	1.03	1.01	1.04	1.03	1.01	1.01	2.11	2.11	1.41	1.41				
	Nd-TPAEN	3.00	1.01	2.22	2.94	2.31	—	0.43	1.05	4.15	—	9.20	1.43	ND	9.20	1.21	4.15	1.72	2.71	4.15	1.72	2.71	2.13	2.13	1.45	1.45						
	Sm-NM	4.64	2.25	15.84	7.31	7.31	—	1.06	2.03	6.69	—	15.63	14.31	40.28	13.50	24.74	39.23	9.64	9.96	39.23	9.64	9.96	8.42	8.42	14.46	14.46						
	Nd-NM	4.94	2.48	16.65	7.54	7.54	—	1.18	2.11	6.88	—	15.81	15.70	42.43	14.41	28.87	41.91	10.07	10.33	41.91	10.07	10.33	8.53	8.53	15.87	15.87						
α_j	Sm-TPAEN	1.03	1.09	1.02	1.01	—	1.13	1.04	1.02	—	1.01	1.03	1.03	ND	1.01	1.02	1.01	1.04	1.03	1.01	1.04	1.03	1.01	1.01	1.01	1.03	1.03					
	Nd-TPAEN	1.55	2.22	5.39	3.16	—	2.50	1.93	1.61	—	1.08	10.01	10.01	ND	11.17	9.98	9.45	5.60	3.67	9.45	5.60	3.67	3.95	3.95	9.94	9.94						
	Sm-NM	1.20	1.10	1.05	1.03	—	1.11	1.04	1.03	—	1.22	1.10	1.10	1.05	1.07	1.17	1.07	1.04	1.04	1.07	1.04	1.04	1.01	1.01	1.10	1.10						
	Nd-NM	0.15	0.04	0.01	0.01	—	0.02	0.02	0.05	—	0.03	0.01	0.01	ND	0.00	0.01	0.01	0.02	0.02	0.00	0.01	0.02	0.01	0.01	0.01	0.01						
R_S	Sm-TPAEN	1.92	0.54	2.88	1.72	—	0.25	0.47	1.38	—	3.41	2.09	2.09	ND	1.99	3.60	5.52	2.14	2.22	1.99	3.60	5.52	2.14	2.22	2.28	2.10						
	Nd-TPAEN	2.49	0.15	0.56	0.16	—	0.07	0.06	0.13	—	0.13	1.14	1.14	1.20	0.84	3.19	2.08	0.37	0.25	0.84	3.19	2.08	0.37	0.25	0.10	1.14						
	Sm-NM	2.49	0.15	0.56	0.16	—	0.07	0.06	0.13	—	0.13	1.14	1.14	1.20	0.84	3.19	2.08	0.37	0.25	0.84	3.19	2.08	0.37	0.25	0.10	1.14						
	Nd-NM	2.49	0.15	0.56	0.16	—	0.07	0.06	0.13	—	0.13	1.14	1.14	1.20	0.84	3.19	2.08	0.37	0.25	0.84	3.19	2.08	0.37	0.25	0.10	1.14						

^a ND: not detected; —: all peaks co-eluted.

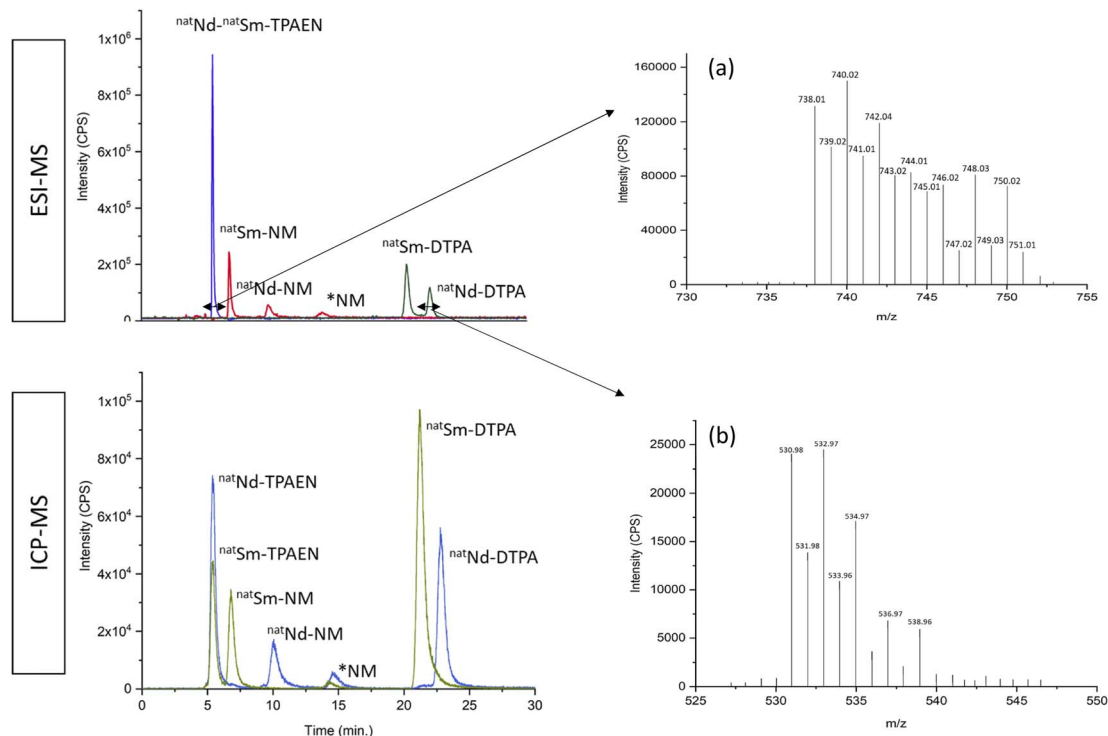


Fig. 2 Chromatograms simultaneously acquired by ESIMS and ICPMS coupled to the separation of the ^{nat}Nd and ^{nat}Sm complexes previously formed with TPAEN, NM and DTPA and mixed in the working mobile phase before the injection. ESIMS spectra were recorded using SIM mode by considering the most abundant m/z ratio of the isotopic pattern of the Ln-complexes, namely $m/z = 743$ for the Ln-TPAEN complexes, $m/z = 702$ for the Ln-NM complexes and $m/z = 537$ for the Ln-DTPA complexes. ICPMS profiles were obtained by registering the signal of the most abundant isotope of ^{nat}Nd ($m/z = 142$) and ^{nat}Sm ($m/z = 152$) (a) Extracted ESI mass spectra of ^{nat}Nd and ^{nat}Sm -TPAEN complexes and (b) extracted ESI mass spectrum of the ^{nat}Nd -DTPA complex. Column: ACQUITY UPLC BEH Amide (150 \times 2.1 mm; 1.7 μm). Mobile phase: 74/26 (v/v) ACN/ H_2O containing 15 mmol L^{-1} $\text{NH}_4\text{CH}_3\text{CO}_2$ and 0.5% formic acid, eluted in isocratic mode. Flow rate: 300 $\mu\text{L min}^{-1}$ and $V_{inj} = 3 \mu\text{L}$. Note: *NM is a ^{nat}Sm and ^{nat}Nd tertiary complex of NM.

the NM complexes and its commercial availability in capillary and nano-flow formats for downscaling of the separation.

3.1.2. Selection of the mobile phase composition. The composition of the mobile phase was adjusted in order to improve the separation performance using the ACQUITY UPLC BEH Amide column. To this end, the acetonitrile content in the mobile phase was increased from 70% to 74 and 76%. As expected, the increase in the ACN content resulted in an increased retention of the complexes, but the ^{nat}Sm and ^{nat}Nd -TPAEN complexes still co-eluted. The best separation of NM complexes was obtained for 74% of ACN, with a resolution factor of around 10 in 25 minutes. The effect of the concentration variation of $\text{NH}_4\text{CH}_3\text{CO}_2$ from 5 to 20 mmol L^{-1} was also evaluated and the best results were obtained for 15 mmol L^{-1} . The separations were also run at temperatures ranging from 22 to 60 $^\circ\text{C}$. This parameter had no significant influence on the separation and a temperature of 40 $^\circ\text{C}$ was chosen for the rest of the experiments (results not shown).

Finally, the best separation conditions were obtained using a mobile phase made of 74/26 (v/v) ACN/ H_2O containing 15 mmol L^{-1} $\text{NH}_4\text{CH}_3\text{CO}_2$ and 0.5% formic acid, eluted in isocratic mode as presented in Fig. 2.

The peaks in the chromatograms registered by ICPMS could be attributed by comparison with the mass spectra extracted

from the peaks of the ESIMS chromatograms, allowing the identification of the associated complexes. For all the chelating molecules, complexes of 1/1 stoichiometry were online observed in agreement with the literature, in which TPAEN complexes were characterized by spectroscopic techniques¹¹ and DTPA complexes using HILIC-ESIMS.^{13,31}

In this study, the HILIC conditions have been set up to separate new sets of Ln complexes formed with hydrophilic synthetic chelating molecules, thanks to an amide functionalized stationary phase. Regarding the studies of Ln species, numerous studies have reported the analysis of Gd-based contrast agents containing DTPA and linear/cyclic poly-aminocarboxylic acid derivatives such as BT-DO3A, DOTA, BMA and BOPTA, by HILIC-ESIMS²⁰ and/or HILIC-ICPMS in blood plasma and urine samples,^{21–23} waters^{23–29} and plants.³⁰ Most of these studies involved zwitterionic-grafted and unmodified silica columns and the separations were generally run in conventional chromatographic format (100–150 mm \times 2–3 mm; 2.6–5 μm).

3.1.3. Downscaling the separation. As previously mentioned, one of the concerns in the nuclear field is the reduction of effluent volumes and the consumption of materials. The initial separation based on the simultaneous coupling to ESIMS and ICPMS was set up to guarantee these premises. In



Table 6 Downscaling parameters associated with the chromatographic separation formats, compared with classical approaches

Format	Classical approach		Our approach		
	Batch ^a		Conventional	Capillary	Nano
Column inner diameter (mm)	—		2.1	0.3	0.075
Flow rate ($\mu\text{L min}^{-1}$)	—		300	5	0.3
Injection volume (μL)	2		3	1	0.05
^{nat} Sm (ng)	—		1.80	0.15	0.015
^{nat} Nd (ng)	—		1.73	0.14	0.014
Eu (ng)	62 600		—	—	—
CM _{total} (ng)	12 000		36.00	2.40	0.24
Effluent volume (mL)/1 h	—		18	0.3	0.018
Total analysis time (min)	—		20	20	25

^a Complexation of Eu by TPAEN was followed by microcalorimetric titrations.¹¹

order to further reduce these parameters, the separation was downscaled by decreasing the inner diameter of the column from 2.1 mm to 300 and 75 μm , involving lower flow rates and sample injection volumes. As a consequence, the mass of ^{nat}Sm and ^{nat}Nd in the injected volume was reduced approximately 12 and 120 times from the conventional format to the capillary and nano-flow formats, and the mass of chelating molecules was accordingly 15 and 150 times lower. Another crucial parameter

is the decreased effluent volumes from 60 to 1000 times per hour, as can be seen in Table 6.

Compared to the determination of the TPAEN affinity for Eu by microcalorimetric titrations described in the literature,¹¹ the total amount of Ln and chelating molecules in the injection volume of our nano-flow method was decreased by around 4×10^6 times and 5×10^5 times respectively, while enabling quantitative data for several molecules complexed by two Ln to be acquired.

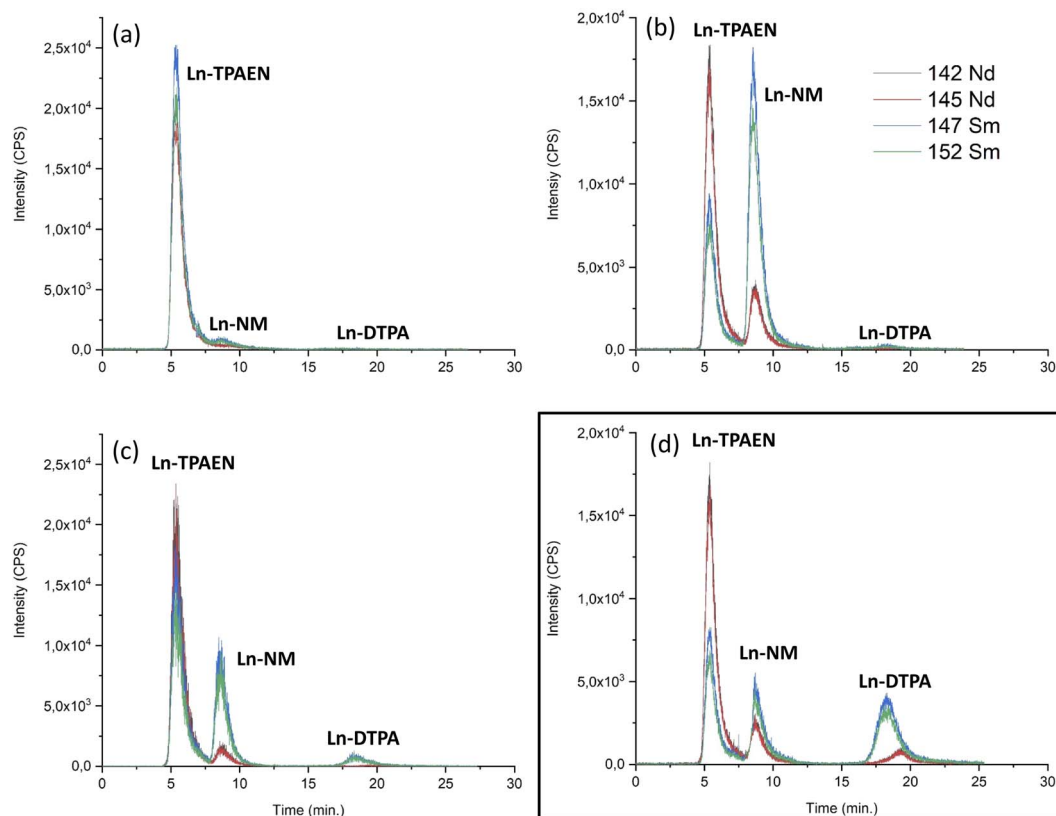


Fig. 3 HILIC-ICPMS chromatograms for the four samples analysed in duplicate. Separations were run in nano-flow format using the conditions presented in Table 4. Composition of the samples as indicated in Table 1: Ln_T : xTPAEN : yNM : zDTPA with (a) 4 : 2.5 : 1.4 : 0.1 (sample 1), (b) 4 : 1.4 : 2.5 : 0.1 (sample 2), (c) 4 : 1.8 : 1.8 : 0.4 (sample 3) and (d) 4 : 1.3 : 1.3 : 1.3 (sample 4).



Table 7 Online measured concentrations of ^{nat}Sm and ^{nat}Nd complexes of TPAEN, NM and DTPA, expressed in $\mu\text{g kg}^{-1}$ and mass balance (%) obtained by summing the ratios of $[\text{Ln}(\text{CM})]$ in the samples and in the controls

Complex	$^{nat}\text{Sm}(\text{CM})$			$^{nat}\text{Nd}(\text{CM})$		
	TPAEN	NM	DTPA	TPAEN	NM	DTPA
Sample 1						
$[\text{Ln}(\text{CM})]_{\text{control}}$	340.9 ($2.3 \times 10^{-6} \text{ mol L}^{-1}$)	323.0 ($2.1 \times 10^{-6} \text{ mol L}^{-1}$)	324.4 ($2.1 \times 10^{-6} \text{ mol L}^{-1}$)	343.6 ($2.3 \times 10^{-6} \text{ mol L}^{-1}$)	333.2 ($2.3 \times 10^{-6} \text{ mol L}^{-1}$)	325.1 ($2.3 \times 10^{-6} \text{ mol L}^{-1}$)
$[\text{Ln}(\text{CM})]_{\text{sample}}$	347.6 ($2.3 \times 10^{-6} \text{ mol L}^{-1}$)	0	0	376.3 ($2.6 \times 10^{-6} \text{ mol L}^{-1}$)	0	0
$\sum(\text{sample/control}) (\%)$	102.0			109.5		
Sample 2						
$[\text{Ln}(\text{CM})]_{\text{control}}$	348.7 ($2.3 \times 10^{-6} \text{ mol L}^{-1}$)	325.7 ($2.2 \times 10^{-6} \text{ mol L}^{-1}$)	323.8 ($2.2 \times 10^{-6} \text{ mol L}^{-1}$)	323.7 ($2.2 \times 10^{-6} \text{ mol L}^{-1}$)	336.9 ($2.3 \times 10^{-6} \text{ mol L}^{-1}$)	325.0 ($2.3 \times 10^{-6} \text{ mol L}^{-1}$)
$[\text{Ln}(\text{CM})]_{\text{sample}}$	157.6 ($1.1 \times 10^{-6} \text{ mol L}^{-1}$)	193.0 ($1.3 \times 10^{-6} \text{ mol L}^{-1}$)	4.4 ($2.9 \times 10^{-8} \text{ mol L}^{-1}$)	272.2 ($1.9 \times 10^{-6} \text{ mol L}^{-1}$)	96.9 ($0.9 \times 10^{-6} \text{ mol L}^{-1}$)	0
$\sum(\text{sample/control}) (\%)$	101.7			102.7		
Sample 3						
$[\text{Ln}(\text{CM})]_{\text{control}}$	349.4 ($2.3 \times 10^{-6} \text{ mol L}^{-1}$)	323.5 ($2.2 \times 10^{-6} \text{ mol L}^{-1}$)	348.7 ($2.3 \times 10^{-6} \text{ mol L}^{-1}$)	340.7 ($2.4 \times 10^{-6} \text{ mol L}^{-1}$)	337.6 ($2.3 \times 10^{-6} \text{ mol L}^{-1}$)	342.5 ($2.4 \times 10^{-6} \text{ mol L}^{-1}$)
$[\text{Ln}(\text{CM})]_{\text{sample}}$	278.4 ($1.9 \times 10^{-6} \text{ mol L}^{-1}$)	93.9 ($6.2 \times 10^{-7} \text{ mol L}^{-1}$)	21.9 ($1.5 \times 10^{-7} \text{ mol L}^{-1}$)	298.9 ($2.1 \times 10^{-6} \text{ mol L}^{-1}$)	32.8 ($2.3 \times 10^{-7} \text{ mol L}^{-1}$)	0
$\sum(\text{sample/control}) (\%)$	105.7			97.4		
Sample 4						
$[\text{Ln}(\text{CM})]_{\text{control}}$	361.7 ($2.4 \times 10^{-6} \text{ mol L}^{-1}$)	375.6 ($2.5 \times 10^{-6} \text{ mol L}^{-1}$)	382.4 ($2.5 \times 10^{-6} \text{ mol L}^{-1}$)	345.6 ($2.4 \times 10^{-6} \text{ mol L}^{-1}$)	349.4 ($2.4 \times 10^{-6} \text{ mol L}^{-1}$)	348.7 ($2.4 \times 10^{-6} \text{ mol L}^{-1}$)
$[\text{Ln}(\text{CM})]_{\text{sample}}$	150.0 ($9.9 \times 10^{-7} \text{ mol L}^{-1}$)	83.9 ($5.6 \times 10^{-7} \text{ mol L}^{-1}$)	149.4 ($9.9 \times 10^{-7} \text{ mol L}^{-1}$)	261.2 ($1.8 \times 10^{-6} \text{ mol L}^{-1}$)	42.3 ($2.9 \times 10^{-7} \text{ mol L}^{-1}$)	28.7 ($1.9 \times 10^{-7} \text{ mol L}^{-1}$)
$\sum(\text{sample/control}) (\%)$	100.7			95.9		

3.2. Online determination of the affinity of TPAEN, NM and DTPA towards ^{nat}Sm and ^{nat}Nd

To meet this aim, various stoichiometric ratios of the three chelating molecules (CMs) were added to ^{nat}Nd and ^{nat}Sm in a competing complexation reaction, as indicated in Table 1. The formed complexes were further separated by HILIC, online identified by ESIMS and simultaneously quantified by ICPMS using the SID. By applying the mass balance, the quantitative distribution of ^{nat}Nd and ^{nat}Sm among the complexes of TPAEN, NM and DTPA could be deduced and the affinity of the CM for each Ln determined.

3.2.1. Online quantitative distribution measurement of ^{nat}Sm and ^{nat}Nd among the TPAEN/NM/DTPA complexes. In the HILIC conditions defined in Section 3.1, very good chromatographic recoveries of ^{nat}Sm and ^{nat}Nd were obtained following each separation run. The recovery percentages of both Ln in all separation formats were between 96 and 106% for TPAEN complexes, 92–104% for NM complexes and 93–107% for DTPA complexes, showing that no Ln remained adsorbed on the stationary phase during the separation process.

The chromatograms obtained by HILIC-ICPMS for the four samples analysed in the nano-flow format are presented in Fig. 3.

The peaks of the Sm and Nd complexes formed with each CM were co-eluted in the nano-flow format compared to the capillary and the conventional formats, even after optimising the composition and elution mode of the mobile phase. It must however be pointed out that this was not an obstacle since ICPMS makes it possible the integration of each individual peak, allowing the quantification of each complex in the different samples.

Samples and controls were subjected to the separation run in duplicate and the complexes were online quantified based on the integration of their total peak area, allowing us to deduce for each of them the $^{nat}\text{Ln}/^{spike}\text{Ln}$ ratio that was used in SID calculations. The measured concentrations of ^{nat}Sm and ^{nat}Nd complexes of TPAEN, NM and DTPA in the samples and controls are summarized in Table 7.

The mass balance (%) of ^{nat}Sm and ^{nat}Nd was calculated by summing the ratios of the complex concentrations obtained by



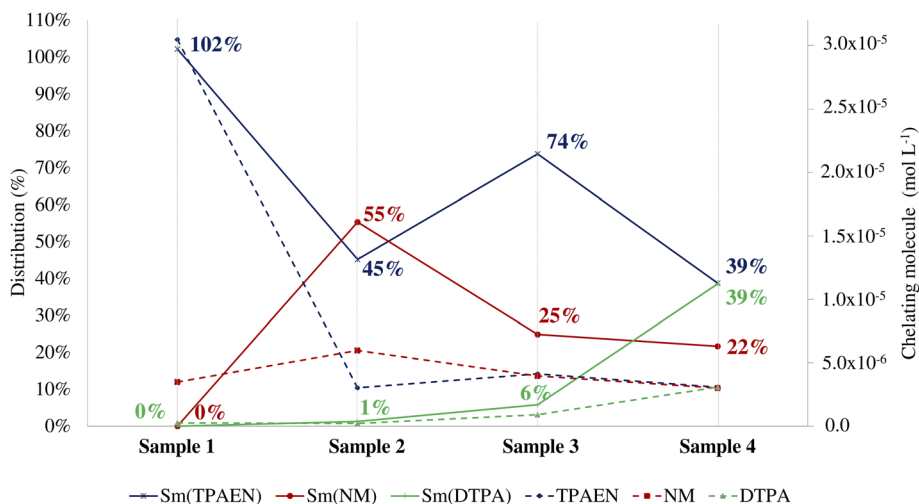


Fig. 4 Quantitative distribution of ^{nat}Sm among the separated complexes depending on the composition of the samples. Ln_T : xTPAEN : yNM : zDTPA: (sample 1) 4 : 2.5 : 1.4 : 0.1, (sample 2) 4 : 1.4 : 2.5 : 0.1, (sample 3) 4 : 1.8 : 1.8 : 0.4 and (sample 4) 4 : 1.3 : 1.3 : 1.3.

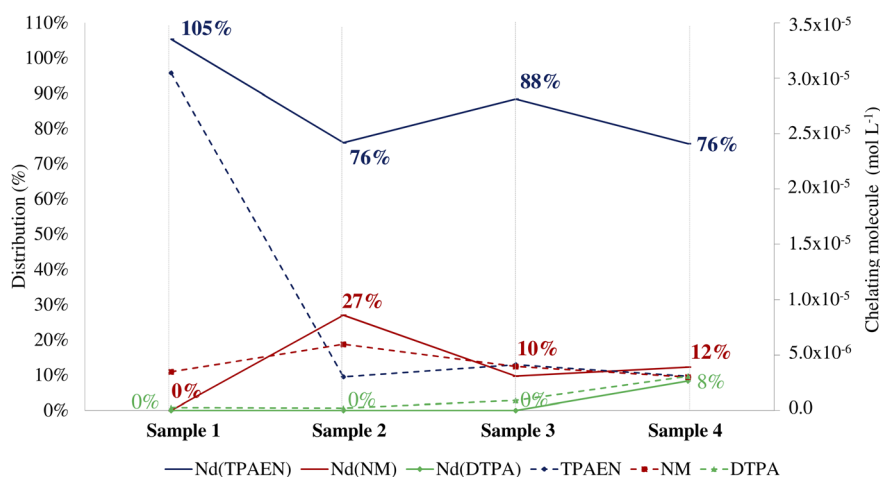


Fig. 5 Quantitative distribution of ^{nat}Nd among the separated complexes depending on the composition of the samples. Ln_T : xTPAEN : yNM : zDTPA (sample 1) 4 : 2.5 : 1.4 : 0.1, (sample 2) 4 : 1.4 : 2.5 : 0.1, (sample 3) 4 : 1.8 : 1.8 : 0.4 and (sample 4) 4 : 1.3 : 1.3 : 1.3.

SID in the samples and the corresponding controls, as shown in (eqn (8)).

$$\sum \text{sample/control (\%)} = \frac{[\text{Ln(TPAEN)}]_{\text{sample}}}{[\text{Ln(TPAEN)}]_{\text{control1}}} + \frac{[\text{Ln(NM)}]_{\text{sample}}}{[\text{Ln(NM)}]_{\text{control2}}} + \frac{[\text{Ln(DTPA)}]_{\text{sample}}}{[\text{Ln(DTPA)}]_{\text{control3}}} \quad (8)$$

The quantitative distribution (%) of ^{nat}Sm and ^{nat}Nd among the separated complexes was obtained by applying eqn (9) and is presented in Fig. 4 and 5 for samples 1–4.

$$\text{Quantitative distribution (\%)} = \frac{[\text{natLn(CMx)}]_{\text{sample}}}{[\text{natLn(CMx)}]_{\text{control}}} \times 100 \quad (9)$$

where ^{nat}Ln is ^{nat}Sm or ^{nat}Nd and CMx for TPAEN, NM or DTPA.

From Table 7, it can be seen that the mass balance of ^{nat}Sm and ^{nat}Nd ranged from 95.9 to 109.5%, which shows that all the chelating molecules fully complexed the Ln.

For samples 1, 3 and 4, when the TPAEN ratio is equal or greater than these of NM and DTPA, ^{nat}Sm is preferentially complexed by TPAEN than by NM, namely 102%, 74% and 39% for ^{nat}Sm(TPAEN) compared to 0%, 25% and 22% for ^{nat}Sm(NM), as can be seen in Fig. 4. In the same samples, 0%, 6% and 39% correspond to ^{nat}Sm(DTPA). For sample 2, when the ratio of NM is 1.8 times higher than that of TPAEN, only 55% was complexed by NM while 45% of ^{nat}Sm was complexed by TPAEN and the DTPA complex was negligible. Regarding sample 4 containing equimolar ratios of the three chelating molecules, ^{nat}Sm is equally distributed under DTPA and TPAEN complexes, being 39% while only 22% is involved in NM complexation.



Table 8 Calculated affinity of CM for intra and inter-group ^{nat}Ln , based on sample 4

Intra-group	^{nat}Sm	^{nat}Nd
$A_{\text{TPAEN-NM}}$	9.9	25.3
$A_{\text{TPAEN-DTPA}}$	4.3	188.5
$A_{\text{NM-DTPA}}$	0.4	7.4
Inter-groups	$^{nat}\text{Nd}/^{nat}\text{Sm}$	
A_{TPAEN}	830.7	
A_{NM}	324.3	
A_{DTPA}	19.0	

For all the samples, ^{nat}Nd is preferentially complexed by TPAEN than NM and DTPA, as can be seen in Fig. 5. In sample 2, when the ratio of NM is 1.8 times higher than this of TPAEN, 76% of ^{nat}Nd remains complexed by TPAEN against 27% by NM and no DTPA complex was formed. Regarding sample 4 containing equimolar ratios of the three chelating molecules, ^{nat}Nd is predominantly complexed by TPAEN (76%) while only around 10% by NM and DTPA.

Overall, when the molecules are present in equimolar ratios (sample 4), TPAEN and DTPA show similar affinity towards ^{nat}Sm and higher than this of NM, while TPAEN exhibits much higher affinity for ^{nat}Nd , reflecting the selectivity of each molecule for the two Ln.

The Ln quantitative distribution among the different complexes calculated for experiments carried out in duplicate for the three separation formats was similar with an RSD < 5%, showing the robustness of the developed analytical method.

3.2.2. Determination of the affinity of TPAEN/NM/DTPA towards ^{nat}Sm and ^{nat}Nd . From a thermodynamic point of view, the complexation constants of a metal ($\log K$ for stepwise reactions and $\log \beta$ for cumulative reactions) are expressed relative to the totally ionized form of the ligands, e.g. DTPA^{5-} where all the carboxylic acid functions (Fig. 1a) are deprotonated. It assures that all constants can be compared. As the acidity of NM is not known, only conditional complexation constants cK , without taking into account the acidity of the functional groups, can be determined and compared to this obtained with the other molecules.

Taking into account the data determined in the previous part, the cK values were calculated for the complexes formed with the three chelating molecules at pH = 1.2 by applying eqn (10), taking $^{nat}\text{Sm}(\text{CM})$ as an example and eqn (10.1) and (10.2) for the calculation of the free proportion of ^{nat}Sm and CM.

$${}^cK^{nat}\text{Sm}(\text{CM}) = \frac{[^{nat}\text{Sm}(\text{CM})]}{[^{nat}\text{Sm}_{\text{free}}][\text{CM}_{\text{free}}]} \quad (10)$$

where CM = TPAEN, NM or DTPA

$$[^{nat}\text{Sm}_{\text{free}}] = [\text{Sm}_{\text{total}}] - ([\text{Sm}(\text{TPAEN})] + [\text{Sm}(\text{NM})] + [\text{Sm}(\text{DTPA})]) \quad (10.1)$$

$$[\text{CM}_{\text{free}}] = [\text{CM}_{\text{total}}] - ([\text{Sm}(\text{CM})] + [\text{Nd}(\text{CM})]) \quad (10.2)$$

In our case, the complexation between the Ln and CM is mostly total, rendering impossible the determination of the thermodynamic complexation constants using the usual representation, according to eqn (11).

$$\log \frac{[\text{Ln}(\text{CM})]}{[\text{Ln}]_{\text{free}}} = \log[\text{CM}]_{\text{free}} + n \log K \quad (11)$$

As $[\text{Ln}]_{\text{free}}$ tends to nil at high CM concentration, the slope of eqn (11) cannot be used.

Nevertheless, the ratio between conditional complexation constants can be used to represent the affinity of one CM towards one Ln. Affinity (A) is the degree to which a substance tends to combine with another, that is, the ratio of conditional complexation constants (cK) between complexes of elements from different groups (inter-groups) or elements within the same group (intra-group). The affinity of one molecule for ^{nat}Nd and ^{nat}Sm , as inter-group elements is represented using eqn (12).

$$A_{\text{CM}} = \frac{{}^cK [\text{Nd}(\text{CM})]}{{}^cK [\text{Sm}(\text{CM})]} \quad (12)$$

In agreement with the trends observed in the previous part, TPAEN presents the highest affinity for ^{nat}Sm compared to this of NM and DTPA, followed by NM having a slightly higher affinity than DTPA (*ca.* 0.4 times). TPAEN exhibits also the highest affinity for ^{nat}Nd with a factor of 25 in relation to NM and 189 when compared to the affinity of DTPA. Finally, NM shows higher affinity for ^{nat}Nd than DTPA (*ca.* 7 times). As can also be seen from the inter-group data, all the CMs exhibit higher affinity for ^{nat}Nd than for ^{nat}Sm , with a factor of 830 for TPAEN, 324 for NM and 19 for DTPA (Table 8). The selectivity and affinity of TPAEN for ^{nat}Sm and ^{nat}Nd follow the same trends observed in the literature, in which this molecule was identified as a potential back-extraction agent for the selective partitioning of Am from nuclear fuel solutions.¹¹ Our method allowed us to determine the affinity and selectivity of NM towards both Ln simultaneously, leading to the conclusion that this latter could be less performant for selective back extraction of Am.

A preliminary study has also been carried out to assess the complexation power of CM for ^{nat}Sm and ^{nat}Nd by increasing the pH of the contact solution, involving different degrees of CM deprotonation according to their pK_a s that are known for DTPA⁵⁴ and TPAEN.¹⁴

Very good mass balance, between 79 and 106% for both ^{nat}Ln , was obtained for the different pH. The quantitative distribution of the ^{nat}Ln among the different complexes in samples containing an equimolar ratio of CM compared to ^{nat}Sm and ^{nat}Nd is shown in Fig. 6. The results were obtained by applying eqn (9).

The results obtained for pH \approx 1 were consistent with the results presented in Fig. 4 and 5. Whatever the pH, TPAEN exhibits the highest complexation ability towards ^{nat}Nd , with



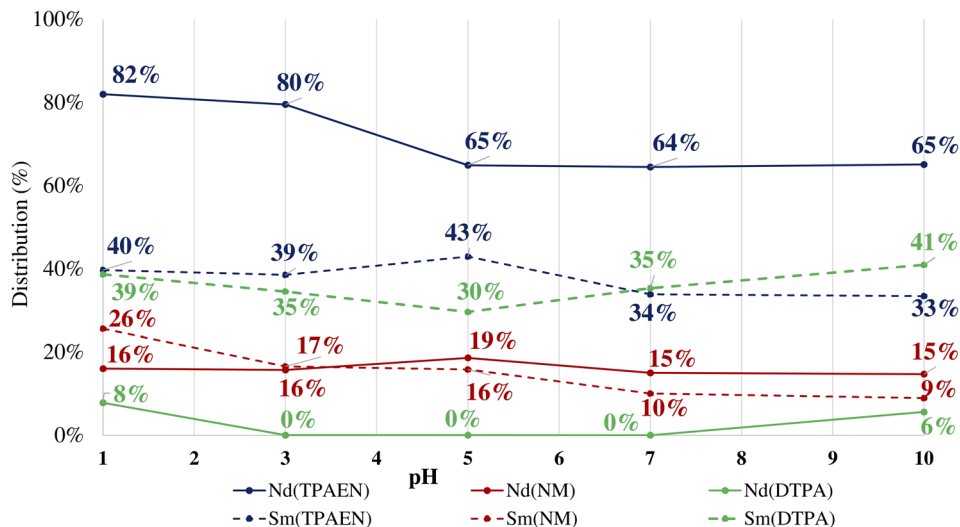


Fig. 6 Quantitative distribution of ^{nat}Nd and ^{nat}Sm among the complexes separated by HILIC-ICPMS under nano-flow conditions reported in Table 4, for two replicates. Sample 4 ($\text{Ln}_T : x\text{TPAEN} : y\text{NM} : z\text{DTPA} = 4 : 1.3 : 1.3 : 1.3$) was prepared at different pH.

82% formation rate of $^{nat}\text{Nd}(\text{TPAEN})$ at $\text{pH} \approx 1$, which decreased to 65% for pH between 5 and 10. In contrast, the pH seems to have no influence on the NM complexation ability of ^{nat}Nd , since the proportion of $^{nat}\text{Nd}(\text{NM})$ ranged between 15 and 19% whatever the pH. The highest formation rate of $^{nat}\text{Sm}(\text{TPAEN})$ was 43% at $\text{pH} \approx 5$ but with small variations for the other pH, between 33 and 40%. The same trend was observed for the $^{nat}\text{Sm}(\text{DTPA})$ complex. The NM complexation ability of ^{nat}Sm was less efficient than those of TPAEN and DTPA whatever the pH, with 26% of $^{nat}\text{Sm}(\text{NM})$ formation rate at $\text{pH} \approx 1$, which undergoes a subsequent decrease to 9% when the pH increased up to 10.

These results show that despite the increase in the pH, involving the deprotonation of the CMs, the trends observed regarding the distribution of the complexes remain similar, with the highest affinity and selectivity of TPAEN for ^{nat}Nd .

5. Conclusion

The objective of the present work was to develop a dedicated method to determine on-line and in a single step the selectivity and the affinity of two hydrophilic synthesized molecules towards ^{nat}Nd and ^{nat}Sm used as analogues of Am and Cm, in comparison with DTPA as a reference molecule. The analytical strategy was based on the simultaneous coupling of HILIC to ESIMS and ICPMS combined with the online quantification of ^{nat}Nd and ^{nat}Sm among the separated complexes by specific isotopic dilution.

The selectivity of several polar stationary phases of commercial columns in conventional format was evaluated and the composition of the mobile phase was adjusted to separate the Ln complexes formed with the three chelating molecules, leading to the selection of the ACQUITY UPLC BEH amide column and a mobile phase made of 74/26 (v/v) ACN/ H_2O , containing 0.5% (v/v) formic acid and $15 \text{ mmol L}^{-1} \text{NH}_4\text{CH}_3\text{-CO}_2$. The separation downscaling from conventional to nano-

flow format allowed us to reduce 120 times the mass of Ln and 150 times the chelating molecules involved in one analysis, as well as a reduction of the effluent volumes by a factor of 1000. This latter format also allowed a significant reduction of chelating molecules and Ln involved in the analysis compared to classical solution chemistry approaches.

The quantification method developed and validated by SID allowed us to quantify online the separated Ln(CM) complexes simultaneously identified by ESIMS, in a single analysis. By applying our approach, the selectivity and the affinity of each chelating molecule for ^{nat}Nd and ^{nat}Sm were determined based on the sample containing stoichiometric ratios of TPAEN, NM and DTPA in competition towards the Ln complexation. In particular, TPAEN exhibits affinity for ^{nat}Nd 830 times higher than for ^{nat}Sm , which is consistent with the selection of TPAEN as a potential selective back-extraction agent in treatment processes dedicated to selective Am partitioning. We could also determine in the same analysis the selectivity and the affinity of NM for ^{nat}Nd and ^{nat}Sm .

This approach can be extended to the online evaluation of the affinity/selectivity of these chelating molecules for the actinides (Pu, Am, Cm...) because of similar physicochemical properties of Ln and An, and by means of an instrumental platform integrated in glove boxes. Moreover, it can be implemented for the screening of the affinity/selectivity properties of various classes of chelating molecules towards elements of interest in the fields of energy, toxicology and environment.

Author contributions

Marina Amaral Saraiva: conceptualization, methodology, investigation, validation, writing – original draft, visualization. Pascal E. Reiller: methodology, validation, writing – review & editing. Cécile Marie: validation, resources – review & editing. Carole Bresson: conceptualization, methodology, validation,



writing – review & editing, supervision, project administration, funding acquisition.

Conflicts of interest

The authors declare that they have no known competing financial interests or personal relationships that could have appeared to influence the work reported in this paper.

Acknowledgements

The authors would like to acknowledge the Nuclear Cycle program (DES-DPE-CYN/PRATA) from the Energy Division of the CEA, the French Alternative Energies and Atomic Energy Commission, for financial support. The authors thank also H el ene Isnard and S ebastien Mialle (DES/ISAS/DRMP/SPC/LANIE) for their help in the qualification and quantification of spike solutions by TIMS.

References

- 1 C. Poinssot, C. Rostaing, S. Grandjean and B. Boullis, Recycling the actinides, the cornerstone of any sustainable nuclear fuel cycles, *Procedia Chem.*, 2012, 7, 349–357, DOI: [10.1016/j.proche.2012.10.055](https://doi.org/10.1016/j.proche.2012.10.055).
- 2 P. Matveev, P. K. Mohapatra, S. N. Kalmykov and V. Petrov, Solvent extraction systems for mutual separation of Am(III) and Cm(III) from nitric acid solutions. A review of recent state-of-the-art, *Solvent Extr. Ion Exch.*, 2020, 39(7), 679–713, DOI: [10.1080/07366299.2020.1856998](https://doi.org/10.1080/07366299.2020.1856998).
- 3 S. Gracia, G. Arrachart, C. Marie, S. Chapron, M. Miguiriditchian and S. Pellet-Rostaing, Separation of Am(III) by solvent extraction using water-soluble H4tpaen derivatives, *Tetrahedron*, 2015, 71(33), 5321–5336, DOI: [10.1016/j.tet.2015.06.015](https://doi.org/10.1016/j.tet.2015.06.015).
- 4 P. Weßling, M. Maag, G. Baruth, T. Sittel, F. S. Sauerwein, A. Wilden, G. Modolo, A. Geist and P. J. Panak, Complexation and Extraction Studies of Trivalent Actinides and Lanthanides with Water-Soluble and CHON-Compatible Ligands for the Selective Extraction of Americium, *Inorg. Chem.*, 2022, 61(44), 17719–17729, DOI: [10.1021/acs.inorgchem.2c02871](https://doi.org/10.1021/acs.inorgchem.2c02871).
- 5 Y. Wang, G. J.-P. Deblonde and R. J. Abergel, Hydroxypyridinone Derivatives: A Low-pH Alternative to Polyaminocarboxylates for TALSPEAK-like Separation of Trivalent Actinides from Lanthanides, *ACS Omega*, 2020, 5, 12996–13005, DOI: [10.1021/acsomega.0c00873](https://doi.org/10.1021/acsomega.0c00873).
- 6 E. Macerata, E. Mossini, S. Scaravaggi, M. Mariani, A. Mele, W. Panzeri, N. Boubals, L. Berthon, M.-C. Charbonnel, F. Sansone, A. Arduini and A. Casnati, Hydrophilic Clicked 2,6-Bis-triazolyl-pyridines Endowed with High Actinide Selectivity and Radiochemical Stability: Toward a Closed Nuclear Fuel Cycle, *J. Am. Chem. Soc.*, 2016, 138, 7232–7235, DOI: [10.1021/jacs.6b03106](https://doi.org/10.1021/jacs.6b03106).
- 7 C. Adam, B. B. Beele, A. Geist, U. M ullich, P. Kaden and P. J. Panak, NMR and TRIFS studies of Ln(iii) and An(iii) C5-BPP complexes, *Chem. Sci.*, 2015, 6(2), 1548–1561, DOI: [10.1039/C4SC03103B](https://doi.org/10.1039/C4SC03103B).
- 8 T. S. Grimes, C. R. Heathman, S. J. Popova, A. S. Ivanov, S. Roy, V. S. Bryantsev and P. R. Zalupski, Influence of a Heterocyclic Nitrogen-Donor Group on the Coordination of Trivalent Actinides and Lanthanides by Aminopolycarboxylate Complexants, *Inorg. Chem.*, 2018, 57(3), 1373–1385, DOI: [10.1021/acs.inorgchem.7b02792](https://doi.org/10.1021/acs.inorgchem.7b02792).
- 9 M. Audras, L. Berthon, C. Berthon, D. Guillaumont, T. Dumas, M.-C. Illy, N. Martin, I. Zilbermann, Y. Moiseev, Y. B. Eliyahu, A. Bettelheim, S. Cammelli, C. Hennig and P. Moisy, Structural Characterization of Am(III) and Pu(III)-DOTA Complexes, *Inorg. Chem.*, 2017, 56, 12248–12259, DOI: [10.1021/acs.inorgchem.7b01666](https://doi.org/10.1021/acs.inorgchem.7b01666).
- 10 C. Moulin, B. Amekraz, S. Colette, D. Doizi, C. Jacopin, C. Lamouroux and G. Plancque, Electrospray mass spectrometry for actinides and lanthanide speciation, *J. Alloys Compd.*, 2006, 408–412, 1242–1245, DOI: [10.1016/j.jallcom.2005.04.177](https://doi.org/10.1016/j.jallcom.2005.04.177).
- 11 N. Boubals, C. Wagner, T. Dumas, L. Chan eac, G. Manie, P. Kauffholz, C. Marie, P. J. Panak, G. Modolo, A. Geist and P. Guilbaud, Complexation of Actinide(III) and Lanthanide(III) with H4TPAEN for a Separation of Americium from Curium and Lanthanides, *Inorg. Chem.*, 2017, 56(14), 7861–7869, DOI: [10.1021/acs.inorgchem.7b00603](https://doi.org/10.1021/acs.inorgchem.7b00603).
- 12 C. Rostaing, C. Poinssot, D. Warin, P. Baron and B. Lorraina, Development and Validation of the EXAM Separation Process for Single Am Recycling, *Procedia Chem.*, 2012, 7, 367–373, DOI: [10.1016/j.proche.2012.10.057](https://doi.org/10.1016/j.proche.2012.10.057).
- 13 E. Blanchard, A. Nonell, F. Chartier, A. Rincel and C. Bresson, Evaluation of superficially and fully porous particles for HILIC separation of lanthanide-polyaminocarboxylic species and simultaneous coupling to ESIMS and ICPMS, *RSC Adv.*, 2018, 8(44), 24760–24772, DOI: [10.1039/C8RA02961J](https://doi.org/10.1039/C8RA02961J).
- 14 N. Chatterton, Y. Bretonni ere, J. P ecaut and M. Mazzanti, An Efficient Design for the Rigid Assembly of Four Bidentate Chromophores in Water-Stable Highly Luminescent Lanthanide Complexes, *Angew. Chem., Int. Ed.*, 2005, 44(46), 7595–7598, DOI: [10.1002/anie.200502231](https://doi.org/10.1002/anie.200502231).
- 15 J. Borrini, A. F. Reguillon, M. Lemaire, S. Gracia, G. Arrachart, G. Bernier, X. H er es, C. Hill and S. Pellet-Rostaing, Water Soluble PDCA Derivatives for Selective Ln(III)/An(III) and Am(III)/Cm(III) Separation, *Solvent Extr. Ion Exch.*, 2015, 33(3), 224–235, DOI: [10.1080/07366299.2014.974449](https://doi.org/10.1080/07366299.2014.974449).
- 16 R. G. Pearson, Hard and Soft Acids and Bases, *J. Am. Chem. Soc.*, 1963, 85(22), 3533–3539, DOI: [10.1021/ja00905a001](https://doi.org/10.1021/ja00905a001).
- 17 R. D. Shannon, Revised Effective Ionic Radii and Systematic Study of Inter Atomic Distances in Halides and Chalcogenides, *Acta Crystallogr., Sect. A: Cryst. Phys., Diffr., Theor. Gen. Crystallogr.*, 1976, 32, 751–767, DOI: [10.1107/S0567739476001551](https://doi.org/10.1107/S0567739476001551).
- 18 K. L. Nash, A review of the basic chemistry and recent developments in trivalent f-elements separation, *Solvent*



- Extr. Ion Exch.*, 1993, 729–768, DOI: [10.1080/07366299308918184](https://doi.org/10.1080/07366299308918184).
- 19 G. T. Seaborg, Overview of the Actinide and Lanthanide (the f) Elements, *Radiochim. Acta*, 1993, **61**, 115–122, DOI: [10.1524/ract.1993.61.34.115](https://doi.org/10.1524/ract.1993.61.34.115).
- 20 J. Künnemeyer, L. Terborg, S. Nowak, A. Scheffer, L. Telgmann, F. Tokmak, A. Günzel, G. Wiesmüller, S. Reichelt and U. Karst, Speciation Analysis of Gadolinium-Based MRI Contrast Agents in Blood Plasma by Hydrophilic Interaction Chromatography/Electrospray Mass Spectrometry, *Anal. Chem.*, 2008, **80**(21), 8163–8170, DOI: [10.1021/ac801264j](https://doi.org/10.1021/ac801264j).
- 21 A. Maia, P. Silva, C. Fernandes, A. Silva, A. L. Barros, D. C. Soares and G. Ramaldes, Chemometric-Assisted Hydrophilic Interaction Chromatographic Method for the Determination of Gadolinium-Based Magnetic Resonance Imaging Contrast Agent in Liposomes, *J. Braz. Chem. Soc.*, 2018, **29**(11), 2426–2440, DOI: [10.21577/0103-5053.20180120](https://doi.org/10.21577/0103-5053.20180120).
- 22 L. Schlatt, A. Köhrer, C. Factor, P. Robert, M. Rasschaert, M. Sperling and U. K. Mild, Dissolution/Recomplexation Strategy for Speciation Analysis of Gadolinium from MR Contrast Agents in Bone Tissues by Means of HPLC-ICP-MS, *Anal. Chem.*, 2021, **93**(33), 11398–11405, DOI: [10.1021/acs.analchem.1c01100](https://doi.org/10.1021/acs.analchem.1c01100).
- 23 S. Feng, S. Shen, Y. Yao, M. Liang, Y. Chen and H. Liu, Comparison of different analytical methods for speciation of seven gadolinium-based magnetic resonance imaging contrast agents and the applications in wastewater and whole blood, *J. Sep. Sci.*, 2022, **46**(4), 2200575, DOI: [10.1002/jssc.202200575](https://doi.org/10.1002/jssc.202200575).
- 24 C. S. Kesava Raju, A. Cossmer, H. Scharf, U. Panne and D. Lück, Speciation of gadolinium based MRI contrast agents in environmental water samples using hydrophilic interaction chromatography hyphenated with inductively coupled plasma mass spectrometry, *J. Anal. At. Spectrom.*, 2010, **25**(1), 55–56, DOI: [10.1039/B919959D](https://doi.org/10.1039/B919959D).
- 25 M. Horstmann, R. Gonzalez de Vega, D. P. Bishop, U. Karst, P. A. Doble and D. Clases, Determination of gadolinium MRI contrast agents in fresh and oceanic waters of Australia employing micro-solid phase extraction, HILIC-ICP-MS and bandpass mass filtering, *J. Anal. At. Spectrom.*, 2021, **36**(4), 767–775, DOI: [10.1039/DOJA00493F](https://doi.org/10.1039/DOJA00493F).
- 26 S. Okabayashi, L. Kawane, N. Y. Mrabawani, T. Iwai, T. Narukawa, M. Tsuboi and K. Chiba, Speciation analysis of Gadolinium-based contrast agents using aqueous eluent-hydrophilic interaction liquid chromatography hyphenated with inductively coupled plasma-mass spectrometry, *Talanta*, 2021, **222**, 121531, DOI: [10.1016/j.talanta.2020.121531](https://doi.org/10.1016/j.talanta.2020.121531).
- 27 M. Birka, C. A. Wehe, L. Telgmann, M. Sperling and U. Karst, Sensitive quantification of gadolinium-based magnetic resonance imaging contrast agents in surface waters using hydrophilic interaction liquid chromatography and inductively coupled plasma sector field mass spectrometry, *J. Chromatogr. A*, 2013, **1308**, 125–131, DOI: [10.1016/j.chroma.2013.08.017](https://doi.org/10.1016/j.chroma.2013.08.017).
- 28 M. Birka, C. A. Wehe, O. Hachmöller, M. Sperling and U. Karst, Tracing gadolinium-based contrast agents from surface water to drinking water by means of speciation analysis, *J. Chromatogr. A*, 2016, **1440**, 105–111, DOI: [10.1016/j.chroma.2016.02.050](https://doi.org/10.1016/j.chroma.2016.02.050).
- 29 L. Telgmann, C. A. Wehe, M. Birka, J. Künnemeyer, S. Nowak, M. Sperling and U. Karst, Speciation and Isotope Dilution Analysis of Gadolinium-Based Contrast Agents in Wastewater, *Environ. Sci. Technol.*, 2012, **46**(21), 11929–11936, DOI: [10.1021/es301981z](https://doi.org/10.1021/es301981z).
- 30 U. Lindner, J. Lingott, S. Richter, N. Jakubowski and U. Panne, Speciation of gadolinium in surface water samples and plants by hydrophilic interaction chromatography hyphenated with inductively coupled plasma mass spectrometry, *Anal. Bioanal. Chem.*, 2013, **405**(6), 1865–1873, DOI: [10.1007/s00216-012-6643-x](https://doi.org/10.1007/s00216-012-6643-x).
- 31 L. Beuvier, C. Bresson, A. Nonell, L. Vio, N. Henry, V. Pichon and F. Chartier, Simple separation and characterization of lanthanide-polyaminocarboxylic acid complexes by HILIC ESI-MS, *RSC Adv.*, 2015, **5**(113), 92858–92868, DOI: [10.1039/C5RA16078B](https://doi.org/10.1039/C5RA16078B).
- 32 B. Buszewski and S. Noga, Hydrophilic interaction liquid chromatography (HILIC)—a powerful separation technique, *Anal. Bioanal. Chem.*, 2012, **402**(1), 231–247, DOI: [10.1007/s00216-011-5308-5](https://doi.org/10.1007/s00216-011-5308-5).
- 33 J. I. G. Alonso and P. Rodriguez-Gonzalez, *Isotope dilution mass spectrometry*, Royal Society of Chemistry, Cambridge, 2013, ch. 1, pp. 1–38.
- 34 P. Rodriguez-González and J. I. García Alonso, Isotope Dilution Mass Spectrometry, *Encyclopedia of Analytical Science*, Elsevier, 3rd edn, 2019, pp. 411–420, DOI: [10.1016/B978-0-12-409547-2.14387-2](https://doi.org/10.1016/B978-0-12-409547-2.14387-2).
- 35 S. Schuhmann and J. A. Philpotts, Chapter 37G Mass-spectrometric stable-isotope-dilution analysis for lanthanides in geochemical materials, in *Handbook on the Physics and Chemistry of Rare Earths*, Elsevier, 1979, vol. 4, pp. 471–481, DOI: [10.1016/S0168-1273\(79\)04016-2](https://doi.org/10.1016/S0168-1273(79)04016-2).
- 36 J. G. Alonso, Determination of fission products and actinides by inductively coupled plasma-mass spectrometry using isotope dilution analysis: A study of random and systematic errors, *Anal. Chim. Acta*, 1995, **312**(1), 57–78, DOI: [10.1016/0003-2670\(95\)00199-A](https://doi.org/10.1016/0003-2670(95)00199-A).
- 37 F. Chartier, M. Aubert, M. Salmon, M. Tabarant and B. H. Tran, Determination of erbium in nuclear fuels by isotope dilution thermal ionization mass spectrometry and glow discharge mass spectrometry, *J. Anal. At. Spectrom.*, 1999, **14**(9), 1461–1465, DOI: [10.1039/a902318f](https://doi.org/10.1039/a902318f).
- 38 M. Bourgeois, H. Isnard, A. Gourgiotis, G. Stadelmann, C. Gautier, S. Mialle, A. Nonell and F. Chartier, Sm isotope composition and Sm/Eu ratio determination in an irradiated ¹⁵³Eu sample by ion exchange chromatography-quadrupole inductively coupled plasma mass spectrometry combined with double spike isotope dilution technique, *J. Anal. At. Spectrom.*, 2011, **26**(8), 1660, DOI: [10.1039/c1ja10070j](https://doi.org/10.1039/c1ja10070j).
- 39 A. Beaumais, A. Nonell, C. Caussignac, S. Mialle, G. Stadelmann, M. Janin, H. Isnard, M. Aubert,



- T. Vercouter and F. Chartier, Determination of the $^{144}\text{Ce}/^{238}\text{U}$ atomic ratio in spent nuclear fuel using double spike isotope dilution mass spectrometry, *J. Anal. At. Spectrom.*, 2022, 37(6), 1288–1297, DOI: [10.1039/D2JA00052K](https://doi.org/10.1039/D2JA00052K).
- 40 A. Gaffney, *Guideline on Isotope Dilution Mass Spectrometry*, Lawrence Livermore National Laboratory, United States, 2017, DOI: [10.2172/1358328](https://doi.org/10.2172/1358328).
- 41 L. R. Snyder, J. J. Kirkland, and J. W. Dolan, *Introduction to Modern Liquid Chromatography*, John Wiley & Sons, Inc., 2009, p. 1, DOI: [10.1002/9780470508183](https://doi.org/10.1002/9780470508183).
- 42 USEPA, U.S. Environmental Protection Agency, *Method 6800: Elemental and Speciated Isotope Dilution Mass Spectrometry*, Washington, DC, 2014, <https://www.epa.gov/sites/production/files/2015-12/documents/6800.pdf>, accessed: 2 August 2023.
- 43 H. Isnard, R. Brennetot, C. Caussignac, N. Caussignac and F. Chartier, Investigations for determination of Gd and Sm isotopic compositions in spent nuclear fuels samples by MC ICPMS, *Int. J. Mass Spectrom.*, 2005, 246(1–3), 66–73, DOI: [10.1016/j.ijms.2005.08.008](https://doi.org/10.1016/j.ijms.2005.08.008).
- 44 F. Chartier, H. Isnard, J. P. Degros, A. L. Faure and C. Fréchet, Application of the isotope dilution technique for ^{93}Zr determination in an irradiated cladding material by multiple collector-inductively coupled plasma mass spectrometry, *Int. J. Mass Spectrom.*, 2008, 270(3), 127–133, DOI: [10.1016/j.ijms.2007.12.005](https://doi.org/10.1016/j.ijms.2007.12.005).
- 45 J. Meija, T. B. Coplen, M. Berglund, W. A. Brand, P. D. Bièvre, M. Gröning, N. E. Holden, J. Irrgeher, R. D. Loss, T. Walczyk and T. Prohaska, IUPAC - Isotopic compositions of the elements 2013 (IUPAC Technical Report), *Pure Appl. Chem.*, 2016, 88(3), 293–306, DOI: [10.1515/pac-2015-0503](https://doi.org/10.1515/pac-2015-0503).
- 46 M. Thompson, S. L. R. Ellison and R. Wood, Harmonized guidelines for single-laboratory validation of methods of analysis (IUPAC Technical Report), *Pure Appl. Chem.*, 2002, 74(5), 835–855, DOI: [10.1351/pac200274050835](https://doi.org/10.1351/pac200274050835).
- 47 NF V03-110-National standards and national normative documents, AFNOR, 2010, <https://www.afnor.org/standard/nfv03-110>, accessed: 2 August 2023.
- 48 K. A. Gschneidner, L. Eyring, G. H. Lander and G. R. Choppin, *Handbook on the Physics and Chemistry of Rare Earths*, Chemistry Elsevier, 1994, vol. 18.
- 49 P. Hemström and K. Irgum, Hydrophilic interaction chromatography, *J. Sep. Sci.*, 2006, 29(12), 1784–1821, DOI: [10.1002/jssc.200600199](https://doi.org/10.1002/jssc.200600199).
- 50 P. Jandera, Stationary and mobile phases in hydrophilic interaction chromatography: a review, *Anal. Chim. Acta*, 2011, 692(1–2), 1–25, DOI: [10.1016/j.aca.2011.02.047](https://doi.org/10.1016/j.aca.2011.02.047).
- 51 A. Leclercq, A. Nonell, J. L. T. Torró, C. Bresson, L. Vio, T. Vercouter and F. Chartier, Introduction of organic/hydro-organic matrices in inductively coupled plasma optical emission spectrometry and mass spectrometry: A tutorial review. Part I. Theoretical considerations, *Anal. Chim. Acta*, 2015, 885, 33–56, DOI: [10.1016/j.aca.2015.03.049](https://doi.org/10.1016/j.aca.2015.03.049).
- 52 A. Leclercq, A. Nonell, J. L. T. Torró, C. Bresson, L. Vio, T. Vercouter and F. Chartier, Introduction of organic/hydro-organic matrices in inductively coupled plasma optical emission spectrometry and mass spectrometry: A tutorial review. Part II. Practical considerations, *Anal. Chim. Acta*, 2015, 885, 57–91, DOI: [10.1016/j.aca.2015.04.039](https://doi.org/10.1016/j.aca.2015.04.039).
- 53 H. P. Nguyen and K. A. Schug, The advantages of ESI-MS detection in conjunction with HILIC mode separations: Fundamentals and applications, *J. Sep. Sci.*, 2008, 31(9), 1465–1480, DOI: [10.1002/jssc.200700630](https://doi.org/10.1002/jssc.200700630).
- 54 R. Smith, A. Martell and R. Motekaitis, *NIST Standard Reference database 46, NIST Critically Selected Stability Constants of Metal Complexes Database Version 8.0*, U.S. Department of Commerce, 2004.

